International Journal of Nanomedicine

Dovepress
open access to scientific and medical research

Open Access Full Text Article

ORIGINAL RESEARCH

Curcumin Transferosome-Loaded Thermosensitive Intranasal in situ Gel as Prospective Antiviral Therapy for SARS-Cov-2

Nermin E Eleraky[1], Mahmoud El-Badry[1], Mahmoud M Omar[2,3], Wesam M El-Koussi[4], Noha G Mohamed[5], Mohamed A Abdel-Lateef[6], Abeer S Hassan[7]

[1]Department of Pharmaceutics, Faculty of Pharmacy, Assiut University, Assiut, Egypt; [2]Department of Pharmaceutics and Industrial Pharmacy, Faculty of Pharmacy, Deraya University, Minia, Egypt; [3]Department of Pharmaceutics and Clinical Pharmacy, Faculty of Pharmacy, Sohag University, Sohag, Egypt; [4]Department of Pharmaceutical Analytical Chemistry, Faculty of Pharmacy, Sohag University, Sohag, Egypt; [5]Department of Pharmaceutical Chemistry, Faculty of Pharmacy, Sphinx University, Assiut, Egypt; [6]Department of Pharmaceutical Analytical Chemistry, Faculty of Pharmacy, Al-Azhar University, Assiut Branch, Assiut, Egypt; [7]Department of Pharmaceutics, Faculty of Pharmacy, South Valley University, Qena, Egypt

Correspondence: Nermin E Eleraky, Department of Pharmaceutics, Faculty of Pharmacy, Assiut University, Assiut, 71526, Egypt, Tel +20 1014017239, Fax +20 (088-002) 2345631, Email Nermineleraky@pharm.aun.edu.eg

Purpose: Immunomodulatory and broad-spectrum antiviral activities have motivated the evaluation of curcumin for Coronavirus infection 2019 (COVID-19) management. Inadequate bioavailability is the main impediment to the therapeutic effects of oral Cur. This study aimed to develop an optimal curcumin transferosome-loaded thermosensitive in situ gel to improve its delivery to the lungs.

Methods: Transferosomes were developed by using 3^3 screening layouts. The phospholipid concentration as well as the concentration and type of surfactant were considered independent variables. The entrapment efficiency (EE%), size, surface charge, and polydispersity index (PDI) were regarded as dependent factors. A cold technique was employed to develop thermosensitive in-situ gels. Optimized transferosomes were loaded onto the selected gels. The produced gel was assessed based on shape attributes, ex vivo permeability enhancement, and the safety of the nasal mucosa. The in vitro cytotoxicity, antiviral cytopathic effect, and plaque assay (CV/CPE/Plaque activity), and in vivo performance were evaluated after intranasal administration in experimental rabbits.

Results: The optimized preparation displayed a particle size of 664.3 ± 69.3 nm, EE% of 82.8 ± 0.02%, ZP of −11.23 ± 2.5 mV, and PDI of 0.6 ± 0.03. The in vitro curcumin release from the optimized transferosomal gel was markedly improved compared with that of the free drug-loaded gel. An ex vivo permeation study revealed a significant improvement (2.58-fold) in drug permeability across nasal tissues of sheep. Histopathological screening confirmed the safety of these preparations. This formulation showed high antiviral activity against SARS-CoV-2 at reduced concentrations. High relative bioavailability (226.45%) was attained after the formula intranasally administered to rabbits compared to the free drug in-situ gel. The curcumin transferosome gel displayed a relatively high lung accumulation after intranasal administration.

Conclusion: This study provides a promising formulation for the antiviral treatment of COVID-19 patients, which can be evaluated further in preclinical and clinical studies.

Keywords: transferosomes, curcumin, in situ gels, coronavirus 2, SARS-CoV-2, intranasal delivery

Introduction

Coronavirus infection 2019 (COVID-19), yielded by the intense acute respiratory illness coronavirus 2 (SARS-CoV-2), is a horrific respiratory condition that led to the present universal pandemic, which was initiated in December 2019.[1,2] Globally, over 630.8 million cases of COVID-19, including over 6.6 million deaths, have been reported by the World Health Organization (WHO) on November 11, 2022,.[3,4] The elevated rate of viral infectivity and medical and diagnostic infrastructure shortages constitute the main hurdles in controlling covid 19 disease. Consequently, research scientists have collaborated with healthcare leads and pharmaceutical corporations to interpret the exact viral structure, infection

Received: 18 June 2023
Accepted: 23 September 2023
Published: 17 October 2023

Graphical Abstract

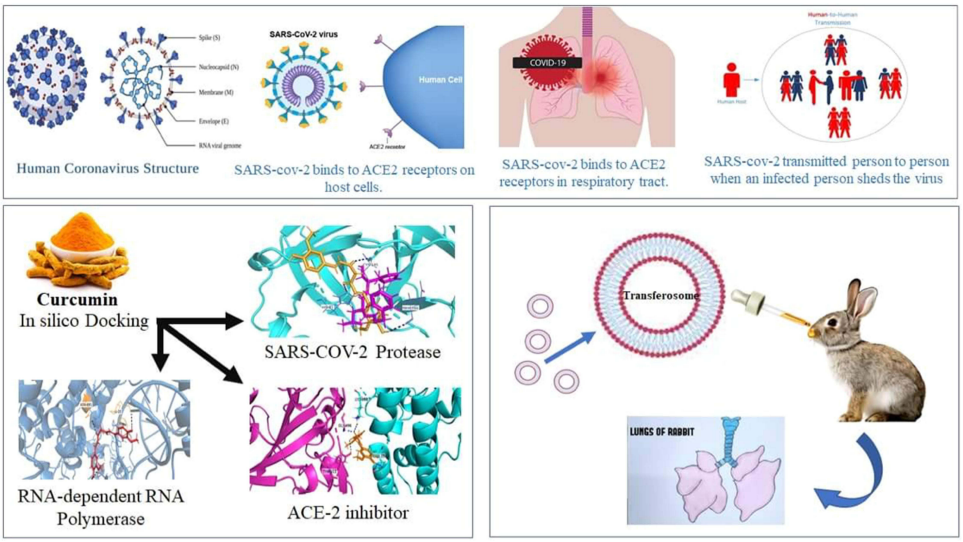

mode, and immunopathogenic mechanisms, and to produce an efficient vaccine and adequate therapeutic alternatives to overcome the pandemic.[2]

SARS-CoV-2 has the largest viral RNA genome, comprising of approximately 30,000 nucleotides. These encode four structural proteins (nucleocapsid (N), membrane (M), spike (S), and envelope (E)) and other nonstructural proteins created as split products to induce transcription and viral replication.[5,6] The life cycle of the virus within the moderator consists of five phases: binding to the host receptors, penetration of the host cells, access of the RNA genome into the nucleus for the replication step, biosynthesis where the mRNA is used to output viral proteins, and eventually, maturation, where the new viruses are created and become free particles.[7] SARS-CoV-2 is transmitted via aerial droplets through direct personal contact.[8]

Fever is the main symptom of COVID-19, in addition to chest pain, difficulty in breathing, sore throat, dry cough, gastric upset, dizziness, diarrhea, vomiting, and nausea.[9] COVID-19 primarily affects the pulmonary system, and some patients progress to acute respiratory distress. Additionally, hypoxemia was recorded in some patients, which may have been due to severe respiratory failure.[10] Furthermore, cardiovascular and neurological symptoms were recorded in certain patients with COVID-19 infection.[11]

The development of efficient therapies for SARS-CoV-2 infection is complicated. Instead, repurposing already licensed pharmaceuticals was considered to develop a fast track to innovate effective treatments for COVID-19. For example, with antimalarial drugs (chloroquine and hydroxychloroquine) and remdesivir,[12] however intense illness was accompanied by treatment with hydroxychloroquine in a random test on COVID-19 subjects in China.[13] The antiretroviral protease inhibitor, lopinavir-ritonavir, was also investigated. However, its clinical effect on SARS-CoV-2 have not yet been verified.[14] Furthermore, managing hypercytokinemia using immunotherapy may be a suitable choice for preventing COVID-19 progress.[15] Convalescent plasma (CP) transfusion is an efficient option; however, plasma should be used within 14 days of recovery.[16] Preventive vaccination strategies include inactivated or live-attenuated vaccines and recombinant vaccines have been developed.[17]

Previous literature reported the damaging effects of SARS-CoV-2 virus infection on the patient's respiratory system, resulting from the dramatic influences on their lung function. Thus, the therapeutic management of COVID-19 infection should involve the control of manifestations affecting the respiratory system and lung functions.[8] During severe COVID-19 illness, the release of large amounts of cytokines may lead to acute respiratory distress syndrome (ARDS), increasing the possibility of developing lung failure and pathological damage.[18] Thus, the demand for a new therapeutic agent is

vital to help cure the infected cases with limited side effects. Nutraceuticals have the potential to boost immunity and minimize inflammatory reactions, thus considered promising to manage the respiratory tract manifestations during COVID-19 infection.[19]

Nanomedicine has attracted attention in different medical fields and is recognized as an essential approach for developing new drug delivery systems for the management of numerous pathological disorders. Natural products loaded within nanocarriers are considered a promising therapy for COVID-19 infections. Nanomedicine could provide various benefits, including the nanocarriers` unique design that enables them to modify physicochemical and pharmacokinetic characteristics of entrapped natural medicinal products.[1] Besides, nano-phytomedicines have attractive attributes that allow them to enhance drug absorption at the biological membranes, provide adequate therapeutic drug concentration with enhanced safety profile evading toxic adverse effects, and improve therapeutic drug bioavailability. Hence, the prospective nanosized drug delivery systems of nutraceutical products could be beneficial for the potential management of COVID-19 infection, respiratory tract symptoms, and lung pathological conditions. Nano vesicles can improve the natural medicinal substances availability by retaining them for a prolonged time, targeting lung and respiratory tract membranes, and achieving controlled release patterns at these absorption sites (respiratory tract and lungs), consequently improving the therapeutic efficacy. Accordingly, nutraceutical nanosystems could be considered promising option for the treatment of COVID-19 infection and provide better recovery with toxicological safety.[1,20] Recently, for more personalized SARS-CoV-2 infection management, nanomedicine could be further tuned to provide effective therapeutic control according to patient medical history and disease status. The personalized therapeutic approach includes the potential use of smart stimuli-responsive nanosystems for controlled drug delivery and release, image-guided nanocarriers to determine the site of drug delivery, magnetic nanocarriers to deliver drugs across body barriers, layer-by-layer approach to deliver multiple drugs to avoid their interactions, or using a patient customized manipulative magnetic nanomedicine, for example, selection of anti-SARS-CoV-2 virus agent (antibody, ARV, CRISPRCas, etc.,) based on patient genomic profiling. The development of personalized therapy should be the focus of future research studies.[1,8]

Among food nutraceuticals, curcumin could be a favorable alternative for therapy and prophylactic of SARS-CoV-2. Curcumin exhibits antiviral efficacy against numerous enveloped viruses, including SARS-CoV-2, through various means, including immediate reaction with membrane proteins of the virus, disorder of the virus outer wrap, blocking of viral proteases, and generation of antiviral host reactions. Additionally, findings from animal models suggest that curcumin supplementation can contribute to the curing and healing of several respiratory diseases, including pulmonary fibrosis, acute obstructive pulmonary illness, pneumonia, sepsis, and acute respiratory distress, by modulating oxidative stress and inflammation.[21] Moreover, curcumin is approved as "Generally Recognized As Safe" by the US Food and Drug Agency.[22]

Wen et al[23] evaluated the therapeutic activities of different phytochemicals against SARS-CoV in Vero 6 cells. They found that certain concentrations of curcumin display considerable anti-SARS-CoV activity. They also found that curcumin inhibited the protease activity of SARS-CoV 3CL, which is necessary for viral replication. Another research group reported a marked decline in IL-6 and IL-1β levels after the treatment of COVID-19 patients with nano curcumin.[24] In latent experimental studies, curcumin was found to reduce lung cell apoptosis, lung injury severity, neutrophils, IL-17A, platelets, and D-dimer levels.[25,26] Zahedipour et al[27] reported the antiviral efficacy of curcumin against COVID-19. However, the authors did not evaluate the biopharmaceutical constraints of this drug and their effects on biological activity.[28]

The insufficient therapeutic effectiveness of curcumin is explained by its low biological availability at the targeted location because of many factors, such as reduced absorption, degradation at physiological pH, fast metabolic reduction and conjugation in the liver, and systemic elimination.[29] Therefore, upon peroral intake, plasma concentrations of curcumin remain undetectable. Many studies are underway to improve the pharmacokinetics of curcumin by innovating preparations to enhance its solubility, absorption, and stability.[30]

Notably, the efficacy of nanoformulations of curcumin, antiviral activity, and potential modes of action against SARS-CoV-2 still need to be evaluated both in vitro and in vivo. Nanotechnology has provided numerous strategies for the repurposing of drugs. These approaches include adjusting pharmacokinetics/pharmacodynamic properties, assuring targeted and controlled drug delivery, lowering systemic toxic effects, and reducing the chance of virus rebound or

lack of medication adherence.[31] Based on nanotechnology, pulmonary delivery of therapeutics is facile using various formulations of nasal sprays, solutions, nebulizers, or gels.[32,33] Pulmonary delivery of curcumin offers several advantages, such as direct delivery of high drug concentration to the location of the infection, immediate curcumin connection with the SARS-CoV-2 virus, instant deposition into the lower airways and alveolar part, and reduced intra- and extracellular detox actions of enzymes in the respiratory tract.[21]

Because of the increased surface area for absorption, rich vascularity, and bypassing of pre-systemic metabolism, drug administration through the nasal cavity is not only convenient, affordable, and non-invasive, but also superior to other routes for improving drug influx.[34] When selecting the most suitable delivery technique to the nasal cavity, it is essential to evaluate the attributes of nanocarriers, such as surface potential, size, and morphology, as they play a vital role in the efficacy and safety of the therapy.[35] The stability of curcumin at the target site would increase due to the nanoformulation's protection from alkaline pH. Additionally, curcumin nanoformulations could offer mucus barrier permeability, sustained release, and longer retention times.[36]

Transferosomes are dispersions of colloidal vesicles mostly composed of nonionic surface-active agents, such as edge activators and phospholipids. Nanovesicles have attracted considerable interest in the field of medication delivery.[37] Transferosomes are extremely deformable vesicles, because edge activators disrupt the connections between phospholipid bilayers, rendering them more elastic. Transferosomes have several benefits, such as biodegradability and biocompatibility, edge activators' capacity to improve the solubility and stability of water-insoluble drugs owing to their surface activity, reduced cytotoxicity, improved drug targeting potential, and capability to extend drug release.[38] According to previously published research, intranasal application of various medications loaded into transferosomes increases their bioavailability.[39,40]

The in situ gel formulations are administered as droplets and then undergo through sol-gel phase transitions at the intended location.[41] Such systems can be converted into gels by altering the temperature, pH, or ionic interactions. At room temperature, thermosensitive in-situ gels are free-flowing, and a temperature change enables the transfer of the solution into a gel. Poloxamers, which are triblock copolymers composed of poly (ethylene oxide)-b-poly (propylene oxide)-b-poly (ethylene oxide), are the most frequently used temperature-sensitive polymers.[42] Controlled and targeted drug delivery can be achieved by embedding vesicular transferosome dispersion into an in situ forming gel base.

The hypothesis of this study was to explore the outcome of the synergistic action between nanotransferosomes drug carriers and in situ gel system as a novel intranasal delivery system of curcumin for maximizing its permeability, bioavailability, and direct transport to the lungs for the efficient management of respiratory conditions resulting from SARS-Cov-2 infection. Transferosomes contain edge activators that can offer enhanced curcumin permeability across the nasal mucosa and an increased drug amount at the absorption site (nasal tissue). Further, this type of nanoplatform shows a small particle size in the nanosized range, thereby providing a higher surface area and improved absorption at the site of action. Besides, loading transferosomes into an in situ gel system offers dual effects: mucoadhesive properties and a controlled drug release pattern. Consequently, it provides an efficient antiviral effect at the pulmonary site and nasal tissue for prolonged periods. The experimental design was applied to evaluate the results of using different types and amounts of edge activators and various lipid concentrations on the characteristics of the prepared curcumin transferosomes. Preliminary experiments were done to identify the range of concentrations of active ingredients. Then, the optimized formulation was selected to formulate an intranasal in situ gel of curcumin transferosomes that was examined for its antiviral action. Previous studies focused mainly on the role of Cur in reducing symptoms and mediating inflammatory responses generated by SARS-Cov-2 infection. However, it is necessary to highlight the advantages of nanosystems that may provide additional features and outcomes in treatment choices based on curcumin. From this perspective, this study evaluates not only the relevant aspects of the investigation of curcumin against SARS-Cov-2 and its mechanisms of antiviral action but also highlights the usefulness of the nanotechnological approach as the means to overcome curcumin biopharmaceutical limitations (low water solubility, and poor bioavailability) and to enable a favorable drug response against SARS-CoV-2.

Accordingly, the main objective of this study was to design a curcumin transferosome-entrapped thermosensitive in situ-forming gel for enhanced drug distribution to the lung through intranasal administration. Curcumin transferosomes were evaluated using a three-factor three-level screening method. The effects of the amount and type of surface-active

agent and lipid amount on the surface charge, entrapment efficiency, hydrodynamic size, and polydispersity index (PDI) were assessed. The optimum formulation of transferosomes was included in poloxamer based in situ gel. The ex vivo permeability and shape of the in situ gel formulations were examined. Antiviral cell-based cytopathic effect and in vitro cytotoxicity assays were also performed. After intranasal administration of the medication to rabbits, an in vivo examination was carried out.

Materials and Methods

Materials

Curcumin (purity > 95%) was purchased from SD Fine-Chem Ltd. (Mumbai India). Phospholipon® 90G was purchased from Lipoid (Steinhausen, Switzerland). Polyoxyl 40 Hydrogenated Castor Oil (Cremophor® RH 40) was obtained from BASF (Monheim, Germany). Span® 60 was obtained from the Adwic El-Naser Chemical Co. (Cairo, Egypt). Gattefosse (Saint-Priest Cedex, France) offered Transcutol® P. BASF (Greenville, OH, USA) provided Poloxamer 407, and Poloxamer 188 (Pluronic® F127, and Pluronic® F68, respectively, triblock copolymers of poly (ethylene oxide)-b-poly (propylene oxide)-b-poly (ethylene oxide)). Tween 80 and Carbopol® 934P (CP 934P) were purchased from Sigma–Aldrich (St. Louis, MO, USA). Spectra/Por ® dialysis membranes (12,000–14,000 molecular weight cut-off) were purchased from Spectrum Laboratories Inc. (Rancho Dominguez, CA, USA). HPLC-grade chloroform and methanol were purchased from Fisher Scientific (Waltham, MA, UK). All Analytical-grade compounds were used as received without further purification.

In silico Docking Study of Curcumin on SARS-COV2 Enzymes

An in silico investigation was conducted to identify the possible mechanisms of action of curcumin on the SARS-COV2 enzymes. The Molecular Operating Environment (MOE 2019.0102, Chemical Computing Group, Montreal, Canada) was used for docking studies. Docking was performed on three enzymes isolated from SARS-CoV-2. These enzymes are the main protease enzymes, RNA-dependent RNA polymerase (RdRp) enzyme, and receptor-binding domain (RBD) of spike protein (S-protein) with human angiotensin-converting enzyme 2 (ACE2). The crystal structures of protease (PDB CODE 7D1M), polymerase co-crystallized with remdesivir (PDB code 7bv2), and the RBD of S-protein with ACE2 (PDB code 6vw1) were downloaded from the protein sequence library. Curcumin was created using the builder features of MOE software. Energy reduction was applied until an RMSD gradient of 0.01 Kcal/mol and RMS range of 0.1 Å with Amber10: EHT force-field attained. The partial charges were automatically estimated. London ΔG was used as a scoring system. PyMOL was used as the visualization program.

Fabrication of Curcumin-Loaded Transferosomes

Curcumin-encapsulated transferosomes were formulated using an established thin-film hydration approach as previously depicted.[43] Briefly, curcumin (20 mg), a surfactant, and phospholipon® 90G were solubilized in a mixture of chloroform and methanol (2:1 v/v) in a circular base flask. A delicate lipid layer was recovered at the base of the round flask following evaporation of the organic mixture (30 min at 40 °C, 900 rpm, and 500 mbar pressure) using a rotary evaporator (Buchi 200; BU CHI Labortechnik AG, Flawil, Switzerland). The thin layer was dried for 4 h in a desiccator to guarantee the total elimination of the organic mixed residues. Artificial nasal fluid (10 mL, SNF, pH 5.5) containing a permeation enhancer (Transcutol® P, 30 mg) was used to hydrate the lipid film. The preparations were vortexed for 2 min and incubated for 2–3 h at ambient temperature to enable complete hydration of the lipid layer. In tightly sealed amber bottles, the prepared transferosomes were maintained at 4 °C until the subsequent experiments.

Experimental Design

A three-factor, three-level screening layout was utilized for the optimization approach via response surface methodology. Table 1 lists the contributing factors and their corresponding levels. The examined parameters were the lipid amount (mg) (A), amount of surfactants (mg) (B), and type of surfactants (Tween 80, Span 60, or Polyoxyl 40 Hydrogenated Castor Oil) (C). Three levels were used to examine each variable: high (+1), moderate (0), and low (−1). These values were

Table 1 Independent and Dependent Variables' Levels Employed in the Factorial Design

Factors	Levels			Responses	Constrains		
	−1	0	+1		Minimum	Maximum	Goal
Lipid amount (mg) (A)	25	50	100	R_1	5.5	97.902	Maximize
Surfactant amount (mg) (B)	7.5	15	30	R_2	202.5	7907	Minimize
Type of surfactant (C)	Tween 80	Span 60	Polyoxyl 40 Hydrogenated Castor Oil	R_3	−8.91	14.1	Minimize
				R_4	0.331	1	Minimize

Notes: A three-factor, three-level experimental design was applied for the optimization approach via response surface methodology. The investigated parameters were the lipid amount (mg) (A), amount of surfactants (mg) (B), and type of surfactants (Tween 80, Span 60, or Polyoxyl 40 Hydrogenated Castor Oil) (C). Three levels were used to examine each parameter: high (+1), moderate (0), and low (−1).

chosen in accordance with preliminary experiments. The responses detected were entrapment efficiency (R1), hydrodynamic size (R2), surface charge (mV) (R3), and PDI (R4).

Data Optimization

Polynomial formulae derived from the exploratory design were employed to adjust the levels of determinants (A, B, and C) to attain the optimal response values of R1, R2, R3, and R4. Optimal preparation was formulated based on the expected values of A, B, and C. The results were estimated and corresponded to anticipated outcomes.

Characterization of Curcumin-Loaded Transferosomes

Particle Size and Zeta Potential

The dynamic laser light scattering (DLS) approach; was used to evaluate the vesicle size distribution of the developed curcumin-transferosomes at 25 °C. A Malvern Zetasizer Nano-ZS (Malvern Instruments, Worcestershire, UK), supplied with a 4mW helium/neon laser operating at (λ = 633 nm) and a temperature sensor was used. Transferosomal suspensions were diluted (30 ×) and vortexed for one minute before each measurement. The particle size values represented in this investigation were equivalent to the hydrodynamic diameters. The surface charge of the transferosomal suspensions was assessed based on electrophoretic mobility data in ultrapure water.[44] Readings were performed in triplicate.

Encapsulation Efficiency

Curcumin encapsulation efficiency (EE%) within the formed transferosomes was calculated via indirect measurement.[45] In Briefly, curcumin-transferosome suspension was subjected to cooling centrifugation (15,000 rpm, 4 °C) for 1 h, utilizing a bench-top centrifuge (large capacity, refrigerated) acquired from Sigma Laborzentrifugen GmbH, Osterode am Harz, Germany). Unincorporated curcumin in the supernatant was measured spectrophotometrically at λ = 430 nm using a Shimadzu model UV-1601 PC (Kyoto, Japan). Encapsulation efficiency (%) was determined using the following equation:

$$EE\% = \frac{WT - WF}{WT} \times 100\%$$

where WT is the weight of the entire curcumin provided and WF is the weight of unencapsulated curcumin measured in the supernatant.

Preparation of Curcumin-Transferosomes in-situ Nasal Gel

Temperature-sensitive in situ forming gelling liquids of Poloxamer 407 in combination with Poloxamer 188 and CP 934P were fabricated using a previously described cold methodology.[46,47] The poloxamer mixture was hydrated in cold SNF (pH 5.5). CP 934P was dispersed in SNF (pH 5.5) and sonicated at 60 °C until swelling. The poloxamer mixture was supplemented with CP 934P dispersion in portions under stirring. To prepare the drug-loaded transferosome gels, curcumin-loaded transferosome suspensions (5 mL, 10 mg curcumin) were mixed with the polymer mixture and treated

as described above. Seven mucoadhesive in-situ nasal gel formulae were fabricated and stored in a cold place (4 °C) for the required evaluations.

Evaluation of Curcumin- Transferosomes in-situ Gels

Clarity and pH

Clearness was assessed visually under suitable lighting, checking for any indications of haziness or the presence of dispersed particulates.[48] The pH of in-situ gel formula was determined at three different temperatures (4 °C, 25 °C, and gelling temperature) using an electronic pH meter (Mettler Toledo, Greifensee, Switzerland). The results are presented as the mean of three measurements with standard deviation.

Measurement of Gelation Temperature ($T_{sol\text{-}Gel}$)

The temperature at which sol-gel transition occurred ($T_{sol\text{-}gel}$) was determined according to a previously described procedure.[49,50] Briefly, cold sample solution (10 mL) was added to a beaker. The aliquot was mixed at 200 rpm with an almost constant rate of temperature increase of ~2 °C/min using a small magnetic bar. The temperature at which the magnet stops spinning, owing to the gelling of the prepared formula, is known as the gelation temperature. $T_{sol\text{-}gel}$ was estimated in triplicate and is displayed as (average ± SD) for each sample.

Rheological Characteristics and Viscosity Data

The viscosity of curcumin transferosomes in-situ forming gels was estimated using a Brookfield digital DV-III viscometer (Brookfield Engineering Laboratories, INC, Stoughton, MA) employing spindle 96, 30 rpm at different temperatures (4 °C, 25 °C, and gelling temperature). The viscosity of each formula was estimated in triplicate and presented as (average ± SD).[51] The rheological characteristics of the curcumin transferosome in situ gels were evaluated. The in-situ gel relative viscosities were assessed at various rates of shear (5–60 rpm), at; 4 °C, 25 °C, and at gelling temperatures. The angular velocity gradually increased when an aliquot was introduced into a small adapter. The rheology of the gel was measured under the same shear rates using Spindle 96, and a rheogram was generated.[41] Triplicate measurements were taken and expressed as the mean ± SD.

Mucoadhesion

The forces of mucoadhesion were assessed for the different in situ gel formulae following previously established protocols.[52] First, 15% (w/v) of mucin-type II was dissolved in SNF (pH 5.5) and allowed to acclimatize for 12 h at 4 °C. The in-situ gelling liquid sample was then heated to 34 °C and blended in a 1:1 ratio with the mucin dispersion after being heated to a similar degree. Prior to testing, the mixture was agitated for 15 min. Finally, using Brookfield digital DV-III equipment, the viscosity values of the in situ gel formulation, mucin dispersion, and in situ gel–mucin mix were estimated (Spindle 96 at 30 rpm). The following equation was used to calculate the increase in the viscosity value post-mucoadhesion.

$$\eta^{b}=\eta^{t}-(\eta^{m}+\eta^{p})$$

where η^{b} denotes the increase in viscosity due to mucoadhesion, η^{t} represents the viscosity of the sample-mucin mix, η^{m} is the viscosity of mucin, and η^{P} is the viscosity of the in situ gel sol. The following equation can be used to estimate mucoadhesive force (F^{b}):

$$F^{b}=\eta^{b}\times\gamma$$

where γ represents the shear rate at which the viscosity was detected.

Drug Content

The amount of drug in the curcumin transferosomes loaded in situ-forming gel was ascertained by dissolving 1 mL of each formulation in methanol (5 mL). Curcumin content was determined spectrophotometrically at λ_{max}= 430 nm using methanol as a blank. Calculations were performed by applying a linear regression analysis formula derived from the standard calibration curve of curcumin in methanol. The average of three measurements was used to determine the mean drug content.

Fourier Transform-Infrared (FT-IR) Spectroscopy

FTIR analysis was used to investigate the chemical features of curcumin powder, curcumin-phospholipon ® 90G-Polyoxyl 40 Hydrogenated Castor Oil physical mixture, freeze-dried plain transferosomes, freeze-dried curcumin transferosomes, freeze-dried curcumin in situ gel, freeze-dried blank in situ gel, and freeze-dried curcumin transferosomes in situ gel. Potassium bromide was used to titrate the aliquots. The triturated slurry was then compressed to form thin discs. An FT-IR spectrophotometer (IR-470, Shimadzu, Kyoto, Japan) was used to collect IR spectra in the 400–4000 cm^{-1} range.

Differential Scanning Calorimetry (DSC)

DSC was used to examine the interactions between curcumin and the formulation components. DSC thermograms were obtained using a thermal analyzer (Linseis STA PT 1600, Germany). Samples (3–5 mg) of curcumin powder, freeze-dried curcumin in situ gel, freeze-dried plain in situ gel, and freeze-dried curcumin transferosomes in situ gel were kept in aluminized DSC crucibles and heated. The scanning and flow rates were adjusted to 10 ˚C/min from 30 to 250 ˚C, and 40 mL/min, respectively. The melting temperature, enthalpy (ΔH, J/g), and onset degree were estimated Using Linseis Evaluation Software.

Morphology

Microscopic images of the optimized curcumin transferosome-laden in situ gel formulation and curcumin transferosome suspension were captured using scanning electron microscopy (SEM, JSM-5400 LV, JEOL, Tokyo, Japan). An aluminum specimen holder was used to retain the samples, which were subsequently dried. Ion sputtering was used to apply a gold coating on the dried samples. SEM was performed at an accelerating voltage of 15 kV.

In vitro Drug Release Assessment

This test was performed to examine the penetration of curcumin from the developed formulations through the synthetic barrier. Drug release from optimum curcumin transferosomes within an in situ forming gel relative to the free curcumin-laden gel, free drug dispersion, and curcumin transferosome dispersion was conducted as explained formerly.[53,54] The accurate weight of the experimented in-situ formed gel samples (1 gram, 0.5 mg curcumin); or 1 mL of either free drug dispersion or optimum curcumin loaded transferosomes dispersion; was put into the donor compartment above a hydrated membrane (Spectra/Por® dialysis cellulose membrane, MW cut off 12–14 kDa) held at the bottom ending of a glass cylinder. The cylinder was immersed in a beaker filled with SNF (pH 5.5, 50 mL + 5% Tween 80). The cells were maintained at 37 ± 0.5 ˚C and 50 rpm in an automatic shaking bath (Gesellschaft für Labortechnik GmbH, Burgwedel, Germany). Samples (3 mL) were collected at scheduled intervals for up to 48 h and replaced with release media. A UV-visible spectrophotometer was used to measure curcumin concentration at λ_{max} = 430 nm. In vitro release tests were performed in three separate runs. Drug release kinetics were inferred from the formulae provided using mathematical modeling techniques (zero-order, first-order, Higuchi, and Korsmeyer-Peppas).[55,56]

Ex vivo Nasal Permeation Investigation

Nasal tissues were used as biological barriers to test the drug permeability. The nasal cavity was extracted from a local slaughterhouse to acquire nasal tissues. The nasal membrane was fixed to the bottom of a glass cylinder. The cylinder was submerged in SNF (pH 5.5, 50 mL + 5% Tween 80) filled beaker. The donor cell was loaded with either optimized curcumin transferosomes within in-situ gel or free drug entrapped in situ gel formula (1 g, equivalent to 0.5 mg curcumin).[57] The permeation units were maintained in an automatically operated shaker bath at 37 ± 0.5 ˚C, where the agitation rate was adjusted to 50 rpm. At predetermined intervals up to one day, 3 mL samplings were withdrawn and replaced with fresh media. The quantity of curcumin that permeated the membrane was determined spectrophotometrically at λ = 430 nm. The total amount of curcumin transported per unit nasal membrane area (Q_n, mg/cm^2) was plotted against the duration (h) to create permeability curves. The apparent permeability coefficient (P_{app}) was estimated using the following equation:

$$P_{app} = \Delta Q/\Delta t/(C_0 \times A)$$

Where $\Delta Q/\Delta t$ = rate of change of the amount of transported drug versus time, C_0 = starting curcumin concentration in donor cell, and A = surface area of the nasal barrier (ie, 3.14 cm^2). The steady-state flux (J_{ss}, $mg/cm^2 \cdot h$) was estimated using the slope of the linear regression line. An enhancement ratio (ER) was estimated by dividing the P_{app} of curcumin obtained for the explored delivery strategy by the P_{app} of curcumin when applied as a free drug in situ gel to the donor compartment.[58]

Stability Study

Aliquots of the ideal in-situ gel loading curcumin transferosomes were kept in firmly capped autoclavable vials and examined for 60 days at 4 °C, ambient temperature (25 ± 2 °C), and at 40 °C).[59] The appearance, surface pH, viscosity, mucoadhesion force, and medication contents of the samples were examined monthly. At the end of two months, each parameter was compared to the initial value. The stability of the tailored transferosome dispersion was also monitored for two months at 4 °C and 25 ± 2 °C. The parameters tested were EE%, particle size, PDI, and ZP.

Antiviral Activity Against SARS-COV 2 and in vitro Cytotoxicity

MTT Cytotoxicity Assay

To examine the half-maximal cytotoxic concentration (CC50), a stock solution of the developed curcumin transferosome in situ gel formulation was prepared in ddH2O and diluted further with DMEM. The cytotoxicity of the sample was evaluated in VERO-E6 cells using the 3-(4, 5-dimethylthiazol-2-yl)-2,5-diphenyltetrazolium bromide (MTT) assay with slight changes.[60] In brief, the VERO-E6 cells were plated in 96-well plates (100 µL/well, 3×10^5 cells/mL) and then set for 24 h at 37 °C in 5% CO_2. The cells were then exposed to different concentrations of the test substances. That was followed by discarding the supernatant and washing cell monolayers with sterile *1x* phosphate buffer saline (PBS) after 24 h of exposure. MTT reagent (20 µL of 5 mg/mL stock solution) was added to each well and maintained at 37 °C for 4 h subsequently, after the medium was aspirated. The produced formazan crystals were solubilized in acidified isopropanol (0.04 M HCl in absolute isopropanol, 200 µL). A plate reader was used to determine the absorbance of the formazan solutions at λ_{max} = 540 nm and 620 nm as the reference wavelength. The percentage of cell toxicity corresponding to the untreated control cell line was calculated using the following equation:

$$\%\ cytotoxicity = \frac{Absorbance\ of\ untreated\ cells\ -\ Absorbance\ of\ treated\ cells}{Absorbance\ of\ untreated\ cells} * 100$$

The concentration that displayed 50% cytotoxicity (CC50) was calculated from a plot of % cytotoxicity versus test concentration.

Estimation of Inhibitory Concentration 50 (IC50)

Vero-E6 cell lines (2.4×10^4) were dispersed in 96-well plates before overnight incubation at 37 °C with 5% CO2 under humidified conditions. After a single (*1x* PBS), the cell monolayers were inoculated with hCoV-19/Egypt/NRC-03/2020 (GSAID registration number: EPI_ISL_430820) for 60 min at ambient temperature. A second layer of DMEM (100µL) comprising; various concentrations of the test substance was placed on top of the cell monolayers. After 72 h of incubation at 37 °C in 5% CO2, the monolayers were treated with paraformaldehyde (100 µL, 4%) for 20 min and stained with crystal violet (0.1% in deionized water) for 15 min at ambient temperature. Pure methanol (100 µL/well) was used to dissolve the crystal violet dye. The optical density of the color was determined at 570 nm using a plate reader (Anthos Labtec Instruments, Heerhugowaard, Netherlands). The value of The substance (IC50); required to diminish the viral cytopathic impact (CPE) by 50% in comparison to the viral control was calculated.[61]

In vivo Pharmacokinetic Assessment

Animals

The South Valley University Faculty of Pharmacy's Research Ethical Committee in Qena, Egypt authorized the animal tests (Ref: P.S.V.U.118/22, May 2022). Animal Experiments were conducted in accordance with the international ethical

guidelines for animal care of the United States Naval Medical Research Centre, Unit No. 3, Abbaseya, Cairo, Egypt, accredited by the Association for Assessment and Accreditation of Laboratory Animal Care international (AAALAC international). The adopted guidelines are in accordance with "Principles of Laboratory Animals Care" (NIH publication No. 85–23, revised 1985). The study protocol was approved by members of "The Research Ethics Committee" and by the head of Pharmacology and Toxicology Department, Faculty of Pharmacy, South Valley University, Egypt. Rabbits (1.5 to 2 kg) were obtained from the University Animal Care Centre. The rabbits under examination had access to food and filtered water, and were maintained in chambers at 25 ± 5 °C.

Analytical Determination of Curcumin via Fluorocytometry

For spiked plasma analysis, blood was drawn from healthy rabbits into heparinized vials. To separate the plasma, blood was centrifuged at 4500 rpm for 10 min. The curcumin-free plasma sample (1 mL) was spiked with known concentrations of curcumin (standard solution:10.0 mg/100 mL acetonitrile) in the range of 5–350 ng/mL, vortexed for 2 min, precipitated with two milliliters of acetonitrile before centrifugation at 4500 rpm for 15 min.[62,63] The fluorescence emission of the supernatant was monitored at $\lambda_{emission}$ =511 nm after $\lambda_{excitation}$ at 423 nm using a spectrofluorometer (FS-2 (Scinco, Korea) fitted with a Xe arc lamp of 150 W, 400 voltage, and a scanning range of 570 nm min-1. The monochromators were set to slit widths of 10 nm. A calibration curve was constructed. The detection and quantification limits (LOD and LOQ, respectively) of curcumin were computed using the following equation:

$$LOD = \frac{3.3 \times S_a}{b}$$

$$LOQ = \frac{10 \times S_a}{b}$$

Where S_a represents the SD of the intercept and b symbolizes the slope.

Protocol of the Animal Study

The pharmacokinetics of the curcumin transferosome-loaded in situ gel formulation was evaluated and compared with those of free curcumin-entrapped in situ-forming gels. The study included two animal groups (n=6; 3 rabbits per group). Each rabbit was administered a curcumin intranasal dose of 5 mg/kg body weight after anesthesia. The first group received curcumin transferosome-loaded in situ gel formulation and the second group received free curcumin-loaded in situ gel preparation. The evaluated formulation (500 µL) was introduced into each nostril of the rabbit using a Hamilton syringe. Blood aliquots were obtained at predetermined periods for 12 h by retro-orbital venous plexus perforation and stored in heparinized vials. To separate the plasma, blood was centrifuged at 4500 rpm for 10 min. Plasma was maintained at −20 °C till assay.[39,64] One milliliter of each stored plasma sample was transferred into a 2-mL tube, deproteinized with two milliliters of acetonitrile solution, vortexed for 2 min, and centrifuged at 4500 rpm for 15 min to estimate the amount of drug in plasma, as previously described in the analytical determination procedures. The fluorescence emission of the supernatant solution was determined at a $\lambda_{emission}$ of 511 nm after $\lambda_{excitation}$ at 423 nm using a fluorescence spectrometer (FS-2 (Scinco, Korea). The pharmacokinetic parameters, including maximum plasma concentration (C_{max}), peak concentration time (T_{max}), area under the concentration-time curve (AUC), plasma clearance (CL), half-life ($t_{1/2}$), and mean residence time (MRT), were studied by non-compartmental analysis using PK solver add-in software in Microsoft Excel.[65] For the biodistribution study, the organs (liver, lung, heart, trachea, kidney, and brain) were separated from euthanized rabbits after 3 and 12 h of treatment. The tissues were washed with normal saline, weighed, minced with scissors, homogenized in phosphate buffer, and centrifuged for 20 min at 4500 rpm.[66] Curcumin was extracted using a previously described method.

Histopathological Study

This study was performed to record any modifications in the integrity of nasal tissue after application of the developed formulation. Nasal tissues of rabbits previously used in pharmacokinetic tests, following 12 h of application of either free drug or drug transferosomes in situ gel formulations, were examined. Excised rabbit nasal mucosa was isolated and

stored in 10% formalin. Dehydration was performed using a graduated alcohol series, followed by the addition of methyl benzoate. The treated samples were then embedded in paraffin wax. Histological evaluation was conducted using a digital imaging light microscope (Nikon Eclipse 80i, Kanagawa, Japan) after isolating and staining numerous sections (four microns) with hematoxylin and eosin dyes. An untreated nasal mucosal sample was used as the control.[67]

Statistical Analysis

Three independent runs were conducted for each test. Outcomes were recorded as the mean ± SD. Statistically significant variations among the various sets were evaluated using one-way analysis of variance (ANOVA) with Tukey Kramer multiple estimates or two-sided t-tests for pairwise comparisons (GraphPad Prism 6.0; GraphPad, San Diego, CA, USA).

Results and Discussion

In silico Docking Study

The structural details and possible intermolecular interactions of curcumin with specific host enzymes essential for viral entry and multiplication were determined through computational studies. The main protease enzyme, RNA-dependent RNA polymerase enzyme (RdRp), and receptor-binding domain (RBD) of the spike protein (S-protein) with human angiotensin-converting enzyme 2 (ACE2) were used to investigate the molecular docking outcomes of curcumin. Previously, GC-376 was reported to inhibit SARS-COV2 replication by targeting the virus main protease.[68] It loses a bisulfite group and binds to cysteine 145 in the catalytically active site via a strong covalent bond, in addition to several hydrogen bonds with the amino acid glutamic 166.[68] Docking of curcumin with the SARS-CoV-2 main protease indicated that curcumin occupies the same active site as GC-376, as shown in Figure 1A and B. It establishes three hydrogen bonds with the amino acids at the binding location. The phenolic OH group of curcumin forms a hydrogen bond with glutamic 166 at the S1 site. A hydrogen bond is formed between one carbonyl group and cysteine 145, whereas the other carbonyl group forms a hydrogen bond with histidine 41. Hydrophobic interactions between threonine 26 and threonine 25 are formed by phenolic rings. The FDA authorized remdesivir to manage SARS-CoV-2 respiratory syndrome.[69] It inhibits viral replication via its action on the viral RNA-dependent RNA polymerase (RdRp) enzyme.[70] Remdesivir covalently binds to the uridine base U20, which is essential for its inhibitory activity.[70] In addition, it forms many hydrogen bonds with U10 and the amino acids Asn 691 and Asp 760. Docking of curcumin into the viral RNA-dependent RNA polymerase (RdRp) enzyme co-crystallized with remdesivir showed that curcumin occupies the same active site as remdesivir, as depicted in Figure 2A-D. The phenolic OH group of curcumin acted as a donor for hydrogen bonding with the key uridine base U20. In addition, two additional hydrogen bonds were formed with the amino acids, asparagine 691 and methionine 542 through ketonic carbonyl and phenolic OH groups, respectively. Curcumin may have

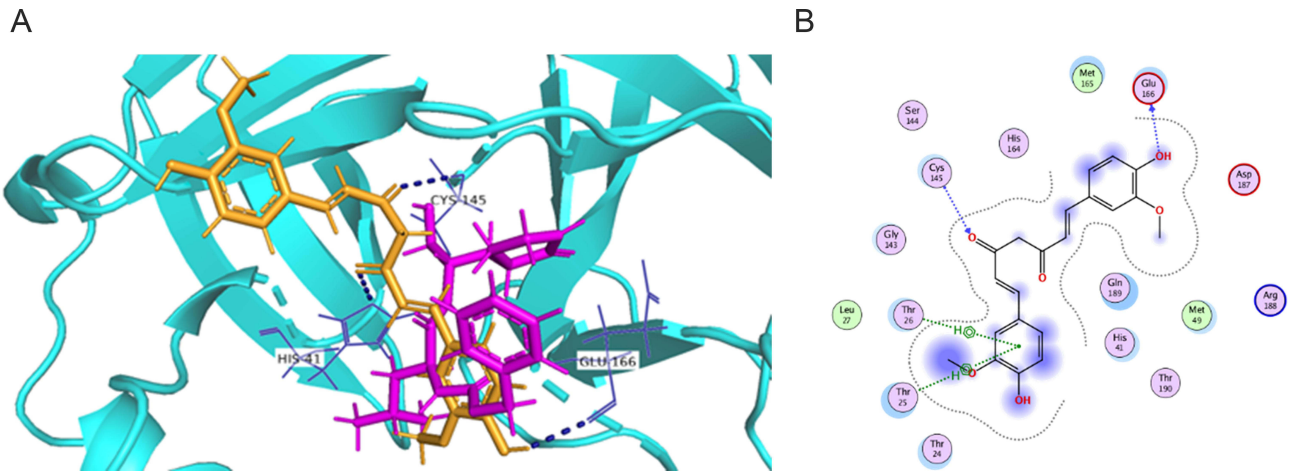

Figure 1 (**A**) Curcumin (in bright Orange sticks) docked on main protease enzyme (cyan cartoon) and overlapped with GC-376 (in mauve sticks). H-bond interactions formed with protease amino acids are shown in blue dots. (**B**) interactions of curcumin with SARS-CoV-2 main protease.

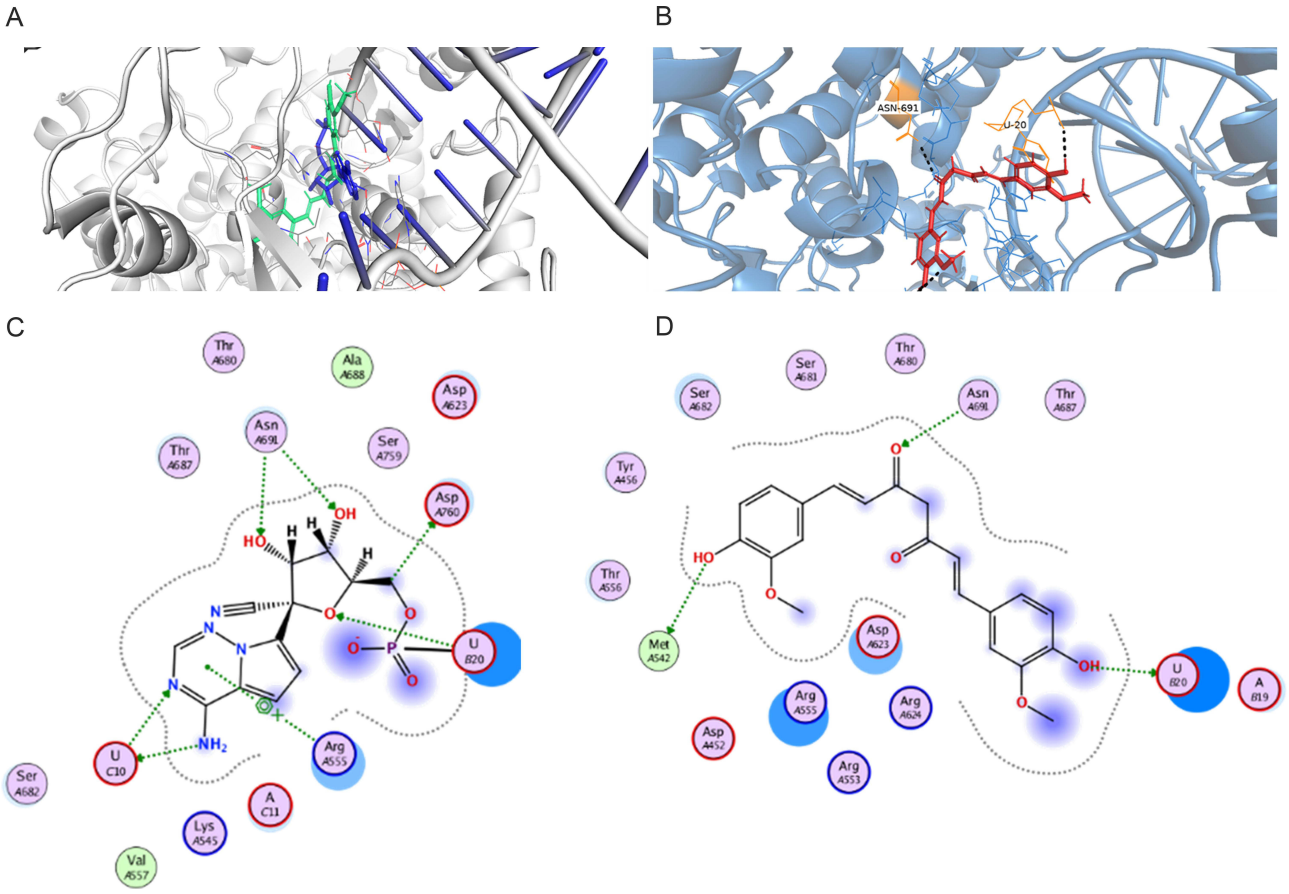

Figure 2 (**A**) Overlay of curcumin (lime green sticks) and remdesivir (blue sticks) in the RNA dependent RNA polymerase PDB code 7bv2. (**B**) docking of curcumin in (RdRp) PDB code 7bv2. (**C**) 2D illustration of the interaction mode of remdesivir on RNA dependent RNA polymerase PDB code 7bv2. (**D**) 2D illustration of the mode of binding of curcumin on RNA dependent RNA polymerase PDB code 7bv2.

an inhibitory effect on viral replication, based on the bonds formed with the active site of the virus (RdRp). A crucial step for the virus' entry into the host cell is the viral spike protein's recognition of the angiotensin converting enzyme 2 (ACE2).[71] According to previous reports, lysine 353 and 31 in the ACE2 enzyme are hotspots for attachment of the virus to the enzyme.[72–74] As shown in Figure 3A glycine 502 and glycine 496 in the virus's receptor-binding domain (RBD) bind to lysine 353, while glutamic 493 interacts with glutamic acid 35 and lysine 31. Docking of the RBD of SARS-CoV-2 complexed with ACE2 revealed that curcumin prevents the interaction between the viral RBD and hotspots of ACE2. Instead, curcumin interacted with the essential amino acids in both the RBD and ACE2 (Figure 3B and C). One carbonyl ketone of curcumin acts as a hydrogen bond acceptor, establishing two hydrogen bonds: the first with the hotspot lysine 353 of the ACE2 active site and the second with glycine 496 located in the RBD of the virus. The other carbonyl group of the drug binds via hydrogen bonding with tyrosine 453 in the RBD. Additionally, the carboxylic group of glutamic acid 33 in ACE2 forms a hydrogen bond with the phenolic OH group of curcumin. According to this study, curcumin may be used as a prophylactic medicine to block the essential amino acids in ACE2 and prevent viral recovery of the ACE2 receptor.

Fabrication and Optimization of Curcumin Loaded Transferosomes

Three nonionic surface-active agents (Tween 80, Polyoxyl 40 Hydrogenated Castor Oil, and Span 60) and phospholipids (Phospholipon® 90G) were used for the potential formation of transferosomes. Nonionic surfactants have been approved by the FDA and are used as edge activators to provide optimum elasticity to vesicle membranes. They are less toxic and more compatible than their anionic, cationic, and amphoteric counterparts. Phospholipids have also been used as bilayer-forming agent.[75,76]

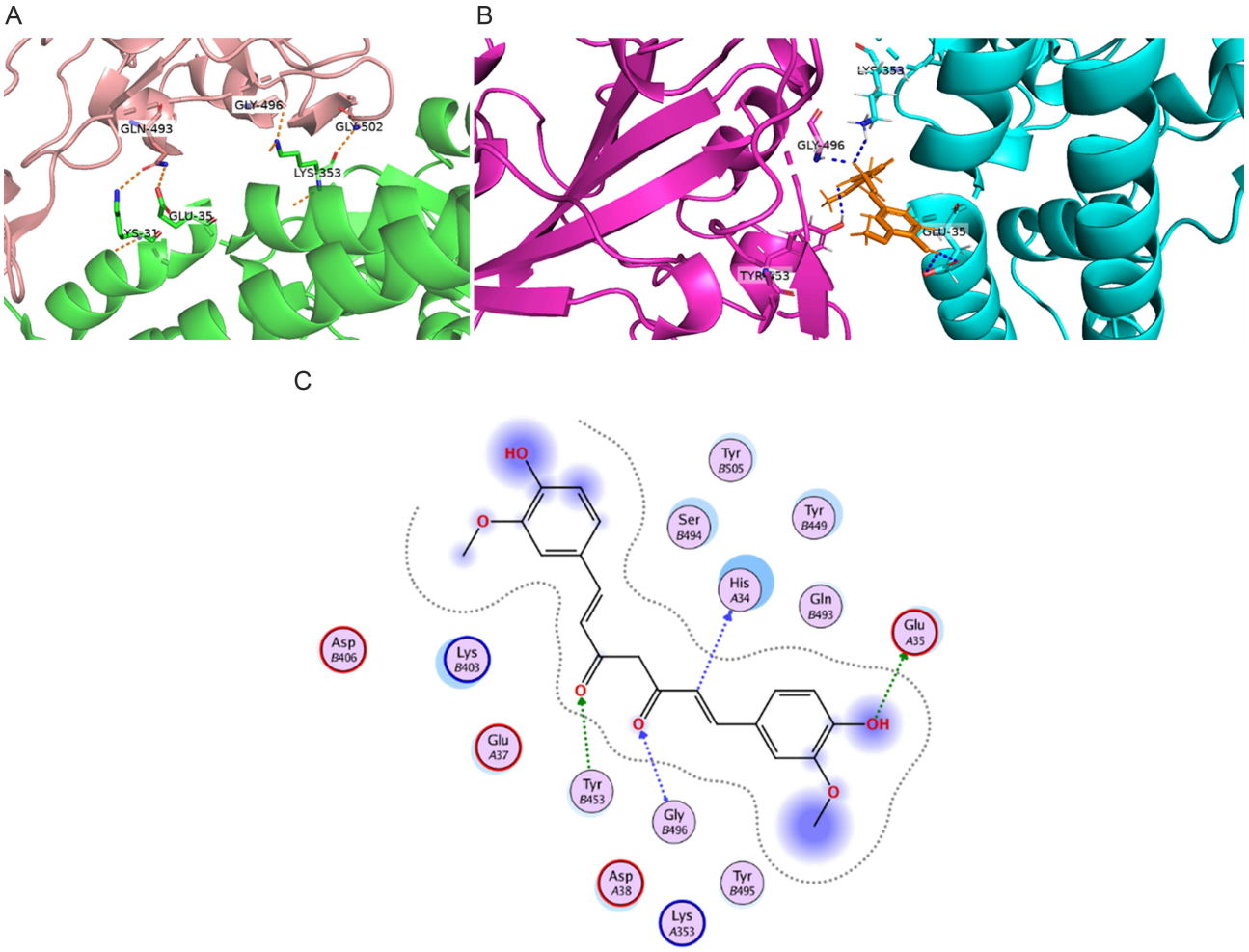

Figure 3 (**A**) binding interactions between RBD of SARS-CoV-2 (shown in salmon) and ACE2 (shown in green). (**B**) curcumin (in Orange sticks) is docked on RBD of SARS-CoV-2 (mauve cartoon) complexed with human ACE2 (cyan cartoon), H-bonds are shown in blue dots. (**C**) 2D representation of the interaction between docked curcumin and SARS-CoV-2 RBD complexed with human ACE2 (PDB code 6vw1).

Factorial Design Analysis

A high-quality product can be fabricated using the design of experiments (DOE) approach, in which various independent factors are applied to examine their effects on various outcomes. According to preliminary investigations, the phospholipid amount, type, and amount of edge activator significantly influence the zeta potential, vesicle size, PDI values, and efficiency of drug entrapment (EE%) of the produced vesicles. Hence, these parameters were chosen for further research into the potential formulation of transferosomes. The Design-Expert® program (version 12.0.0, Stat-Ease Inc., Minneapolis, MN, USA); was used to examine the results generated for each response. The best model with polynomial equations (1–4); was selected. These formulae were used to extract data after evaluating the magnitude and sign of the coefficients. Positive and negative signs denote the synergistic and antagonistic effects, respectively. Data assessment by ANOVA showed that the sequential model proposed for examining the various factors was quadratic for (R1 and R3), and the 2F1 model was proposed for (R2 and R4) response. The Box–Cox plot for particle size suggested a log transformation to satisfy the ANOVA assumption. The analysis confirmed the fit of the generated models with the predicted R-squared values, which were in good agreement with the adjusted values.

$$\begin{aligned} \text{R1 EE} = {} & +93.55 - 1.28\,\text{A} + 0.13\,\text{B} + 2.19\,\text{C}[1] + 1.83\,\text{C}[2] - 17.72\,\text{AB} - 12.68\,\text{AC}[1] - 5.97\,\text{AC}[2] - 16.00 \\ & \text{BC}[1] + 2.73\,\text{BC}[2] - 13.92\,\text{A}^2 - 2.62\,\text{B}^2 \end{aligned} \quad (1)$$

$$\text{Ln (R2 Vesicle size)} = +6.662 + 0.040^{*}\,A - 0.101^{*}\,B + 0.100^{*}\,C[1] - 0.435^{*}\,C[2] - 0.140^{*}\,AB + 0.061^{*}\,AC[1] + 0.274^{*}\,AC[2] + 0.074^{*}\,BC[1] + 0.086^{*}\,BC[2] \quad (2)$$

$$\text{R3 (zeta potential)} = -4.03 - 0.59\,A + 0.14\,B + 0.75\,C[1] + 0.44\,C[2] - 1.81\,AB + 1.72\,AC[1] - 1.18\,AC[2] + 0.12\,BC[1] + 1.15\,BC[2] + 0.77\,A^2 - 1.09\,B^2 \quad (3)$$

$$\text{R4 PDI} = +0.63 - 0.009734\,A - 0.016\,B + 0.011\,C[1] - 0.11\,C[2] - 0.030\,AB + 0.065\,AC[1] + 0.043\,AC[2] + 0.049\,BC[1] - 0.003964\,BC[2] \quad (4)$$

The significance of the different factors was illustrated using ANOVA (Table S1). The obtained data indicated that the interaction of AB, AC, and BC_1 (Tween 80) antagonistically influenced the EE%, with a p-value < 0.0001. The interaction influence of BC_2 (Polyoxyl 40 Hydrogenated Castor Oil) positively affected EE% (p-value < 0.0001). The expected R-squared value (0.754) agreed with the adjusted R-squared value (0.8164) and the variation was lower than 0.2. The signal-to-noise ratio was estimated with adequate precision, and a ratio of at least 4 was preferred. The observed ratio of 17.650 indicated a strong signal. Therefore, this model can be used to explore the layout space. The amount of lipids positively influenced the particle size (p = 0.037). The amount of surfactant negatively affected particle size (p = 0.012). The type of surfactant (Tween 80) affected the particle size synergistically, whereas Polyoxyl 40 Hydrogenated Castor Oil had an antagonistic effect (p < 0.0001). The interaction between AC and BC showed a significant synergistic effect on the particle size (p < 0.0001 and p = 0.04, respectively). AB showed significant antagonistic effects on vesicle size, with a p-value of 0.017. The anticipated and adjusted R-squared values agreed well, with a sufficient degree of precision.

The amount of lipid and the interaction between AB and $AC_{2(\text{Polyoxyl 40 Hydrogenated Castor Oil})}$ negatively affected the vesicle surface charge (p = 0.017, p < 0.0001, and p < 0.0001, respectively). The type of surfactant (Tween 80 and Polyoxyl 40 Hydrogenated Castor Oil) and the interaction between $AC_{1(\text{Tween 80})}$ and BC showed a significant synergistic effect on vesicle potential (p-values of 0.0005, <0.0001, and <0.0001, respectively). The type of surfactant (Tween 80) and the interaction with AC affected PDI synergistically (p < 0.0001 and 0.0001, respectively), while Polyoxyl 40 Hydrogenated Castor Oil exhibited a negative effect on PDI (p < 0.0001). The data supplied by the Design-Expert® program were represented by a 3D response surface plot (Figure 4). The observed responses and the analysis of variance are summarized in Tables 2 and S1.

Influence of Variables on EE%

Encapsulation efficiency (EE%) measurement is vital for determining the amount of curcumin that can be encapsulated into transferosomes for preferable drug encapsulation, extended circulation time, controlled release, and protection.[38] Except for F17& F19, all the prepared curcumin transferosomes displayed a satisfactory EE%, with values varying from (79.546 ± 1.026%) for F9 to (97.694 ± 0.198%) for F20 (Table 2). The generation of mixed micelles with reduced drug entrapment capability may be caused by the decrease in encapsulation efficiency of transferosomes made with Tween 80, resulting from the increase in surfactant concentration.[77] In addition, a high surfactant concentration results in enhanced vesicle membrane permeability and destabilization of the Phospholipon® 90G bilayer, which could create pores within the membrane of vesicles, causing more fluidity and immediate expulsion of the loaded drug.[78–80] The interaction between the edge activator type and concentration was synergistic in the case of Polyoxyl 40 Hydrogenated Castor Oil - based transferosome preparations compared to those prepared using the Tween 80 surfactant. This result can be explained by the saturated nonbranched chain present in the Polyoxyl 40 Hydrogenated Castor Oil structure, which may help stabilize the nanovesicles and improve drug entrapment. Tween 80, on the other hand, exhibited more steric arrangement. There was insufficient area on the vesicle surface to be occupied at higher concentrations of Tween 80.[81,82] Additionally, as reported in the literature, higher concentrations of surfactants increase the vesicle formation number, leading to an increase in the hydrophobic bilayer zone volume, which is useful for entrapping lipophilic therapeutics. The optimal amount of surfactant added to the preparation was determined by the surfactant-phospholipid interaction and density at which the phospholipids were packed.[79] The significant antagonistic effect (p < 0.0001) of the amount of lipid (A^2) on

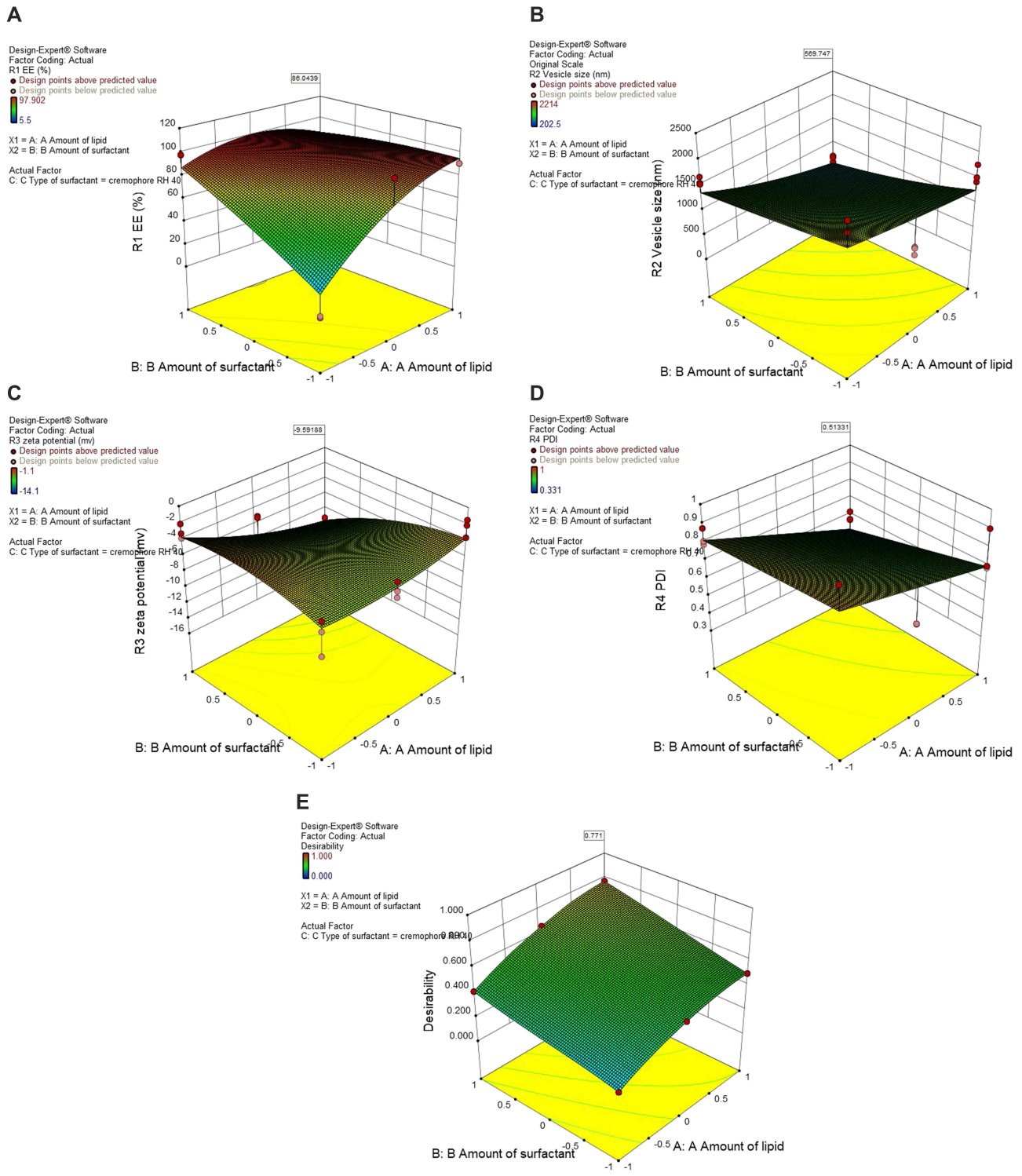

Figure 4 Three-dimensional response surface plots, representing the effect of lipid amount (**A**) and surfactant amount (**B**) on (**A**) entrapment efficiency (EE%), (**B**) vesicle size, (**C**) zeta potential, (**D**), polydispersity index (PDI) and (**E**) desirability of the prepared transferosomes formulations.

EE% may be explained by the possible contest between curcumin and Phospholipon® 90G in the constituted bilayer, which may lead to drug expulsion and disturbance of the vesicle membrane structure, as previously explained by Ahmed.[83]

Table 2 Experimental Runs and Their Observed Responses

Run	Amount of Lipid (mg) A	Amount of Surfactant (mg) B	Type of Surfactant (C)	EE (%) (± SD)	Vesicle Size (nm) (± SD)	Zeta Potential (mV) (± SD)	PDI (± SD)
1	100	30	Polyoxyl 40 Hydrogenated Castor Oil	82.829 ± 0.023	664.333 ± 69.255	−11.243 ± 2.542	0.587 ± 0.027
2	50	7.5	Polyoxyl 40 Hydrogenated Castor Oil	95.981 ± 0.280	854.967 ± 86.473	−5.5 ± 0.946	0.592 ± 0.002
3	100	7.5	Polyoxyl 40 Hydrogenated Castor Oil	90.501 ± 0.039	1573 ± 175.605	−2.387 ± 1.082	0.763 ± 0.119
4	50	30	Span 60	93.448 ± 0.131	620.2 ± 25.800	−3.18 ± 0.151	0.558 ± 0.010
5	25	30	Tween 80	93.863 ± 0.461	1027.1 ± 232.972	−3.86 ± 0.291	0.723 ± 0.099
6	50	30	Span 60	96.073 ± 0.377	618 ± 24.773	−3.26 ± 0.193	0.549 ± 0.019
7	25	7.5	Tween 80	94.184 ± 0.302	590 ± 8.911	−5.84 ± 1.897	0.446 ± 0.103
8	100	15	Span 60	80.145 ± 0.011	668.4 ± 44.965	−4.6 ± 0.285	0.556 ± 0.008
9	25	7.5	Span 60	79.546 ± 1.026	452.233 ± 12.158	−4.286 ± 0.664	0.574 ± 0.043
10	100	15	Span 60	80.139 ± 0.010	646.7 ± 45.556	−4.88 ± 0.291	0.551 ± 0.010
11	50	7.5	Span 60	80.342 ± 0.197	764.366 ± 21.658	−7.366 ± 0.598	0.625 ± 0.035
12	25	15	Span 60	84.52 ± 0.109	256.4 ± 47.164	−1.283 ± 0.202	0.404 ± 0.012
13	50	15	Tween 80	94.494 ± 0.521	872.033 ± 27.513	−3.086 ± 0.395	0.637 ± 0.057
14	50	15	Tween 80	94.843 ± 0.500	855.8 ± 25.500	−3.16 ± 0.399	0.659 ± 0.060
15	25	15	Span 60	84.42 ± 0.1	276.6 ± 45.1	−1.25 ± 0.200	0.412 ± 0.010
16	100	7.5	Span 60	80.244 ± 0.023	602.733 ± 22	−4.5 ± 1.123	0.523 ± 0.008
17	25	7.5	Polyoxyl 40 Hydrogenated Castor Oil	6.166 ± 0.764	2138 ± 119.716	−6.08 ± 2.087	1 ± 0
18	25	30	Polyoxyl 40 Hydrogenated Castor Oil	97.684 ± 0.157	1582.333 ± 76.944	−3.07 ± 0.881	0.822 ± 0.046
19	100	30	Tween 80	34.541 ± 1.291	695.366 ± 147.532	−3.056 ± 0.483	0.622 ± 0.083
20	100	7.5	Tween 80	97.694 ± 0.198	1333 ± 325.593	−2.133 ± 0.415	0.768 ± 0.160
21	50	30	Polyoxyl 40 Hydrogenated Castor Oil	92.593 ± 0.034	579.033 ± 113.248	−6.44 ± 2.142	0.575 ± 0.036
22	50	15	Tween 80	94.744 ± 0.500	856.5 ± 27.122	−3.44 ± 0.401	0.680 ± 0.055

Influence on Particle Size

The size of the transferosomes formed varied from (256.4 ± 47.164 nm) to (2138 ± 119.716 nm) as shown in Table 2. Curcumin transferosomes developed using Span 60 (lipophilic surfactant, HLB = 4.7) had smaller vesicle sizes than Tween 80-and Polyoxyl 40 Hydrogenated Castor Oil based transferosomes (hydrophilic surface-active agents, HLB = 15, and 14–16, respectively). The decline in the surface free energy accompanying the hydrophobic nature of the surfactant is used to explain the apparent relationship between the surfactant HLB and vesicle size.[84] Correlation findings between the amount of phospholipids and vesicle size showed a significant synergism between the lipid amount and the size of the formed vesicles. This observation might be related to the construction of multilamellar vesicles upon increasing lipid concentration. The same explanation was previously reported by Varia et al[80] and El-Gizawy et al.[85] In previous reports, the larger particle size of vesicles with higher phospholipid amounts was explained by the presence of inadequate drug molecules for full binding and intercalation within the lipid bilayer, which leads to effective cohesiveness among the polar parts of the membrane, thereby minimizing the size of transferosomes.[86,87] In addition, the increased amounts of phospholipids employed in the formulation may result in an increase in the overall number of lipoid particles assembling each vesicle, which is proportional to the particle size.[85,88] The effect of surfactant concentration on the vesicle size was also investigated. Generally, increasing the surfactant amount, carbon chain longitude, and hydrophilic nature of the surfactant head groups leads to a decrease in the vesicle size.[38] When a higher concentration of surfactant (Polyoxyl 40 Hydrogenated Castor Oil) with a high molecular weight and increased surface activity was used, a reduction in the vesicle size was confirmed. This finding can be linked to the high concentrations of the surfactant (greater than 15%) enhanced the formation of micelles rather than the formation of transferosome vesicles.[89] In addition, reduced-sized vesicles may be composed of high concentrations of surfactants because of the large amount of surfactant that coats the surface of nano-lipid particles, which permits the formation of smaller vesicles due to the lowering of the interfacial tension.[90] Polyoxyl 40 Hydrogenated Castor Oil, on the other hand, typically produces large transferosomes when used as an edge activator. This is because Polyoxyl 40 Hydrogenated Castor Oil comprises 40 hydrophilic polyethylene oxide units, consequently increasing the capability of vesicles to absorb water with an appreciable increase in vesicle size.[91] In contrast, the increase in transferosome size with increasing Tween 80 concentration may be attributed to the repulsive interaction between the surfactant and phospholipid bilayers.[79,92] More steric repulsion in the continuous aqueous phase is provided by the multiple ethylene oxide side chains present in the Tween 80 structure.[93]

Effect of Variables on PDI

PDI is an indicator of the consistent distribution of the nano-transferosomes' size. PDI was closer to zero, indicating a higher formulation homogeneity.[94] Except for formulation 17, the PDI values of all formulations were below 1 (Table 2, indicating a relatively consistent size distribution. Consequently, they provide unified vesicles with improved physical tolerability.[85] PDI increased with the interaction between phospholipid amount and either Tween 80 or Polyoxyl 40 Hydrogenated Castor Oil surfactants. Without employing a size-lowering procedure, the thin-film hydration technique for producing multilamellar vesicles may contribute to the generation of a relatively large size distribution.[95]

Influence of Variables on ZP

The potential of colloidal particulates in the hydrodynamic shear plane was described by the zeta potential. The increased zeta potential values (regardless of their signs) reflect the colloidal stability.[96] The repulsive action among the vesicles, which prohibits their aggregation, may be responsible for the stability enhancement, resulting in highly stable and consistent dispersion.[97] The zeta potentials of all transferosomes were negatively charged and varied from −1.25 ± 0.200 mV for F15 to −11.243 ± 2.542 mV for F1 (Table 2). Phosphatidylcholine carries both positively (quaternary ammonium) and negatively (phosphate) charged moieties. Above pH3, deprotonation of the phosphate group occurs, imparting a negative charge. In contrast, the quaternary ammonium group is always positively charged irrespective of the medium pH.[98,99] The high negative surface potential may be related to the use of the nonionic surfactant, Polyoxyl 40 Hydrogenated Castor Oil. A fatty acid ester composed of Polyoxyl 40 Hydrogenated Castor Oil is dissociated to form a negatively charged free fatty acid, which imparts a negative charge to vesicles.[100] The potential of Tween 80-containing transferosomes is negative, which is related to the partial hydrolysis of polyethylene oxide head groups.[101] In addition to

the electrical and steric barriers hindering accumulation and improving the physical resilience of the system, negatively charged transferosomes also increase the mucosal permeability of therapeutics.[85,102] Regression assessment demonstrated that BC (type of surfactant × amount) had a synergistic effect on the ZP. The interaction between the amount of surfactant and phospholipid (AB) displayed a significant antagonistic effect on surface charge (Figure 4 and Table S1). In addition, the absolute zeta potential value is affected by the interaction between the amount of lipids and nature of the surfactant (AC). Tween 80 showed a synergistic effect on ZP values, whereas Polyoxyl 40 Hydrogenated Castor Oil negatively affected ZP values. This finding is in agreement with a prior study by El-Gizawy et al,[85] who observed that increasing the Tween 80 concentration increased the value of ZP in the formulated transferosomes. Transferosomes containing Tween 80 displayed steric and electrical hindrance, which inhibited aggregation and enhanced dispersion stability.[103] For transferosomes prepared using a high amount of Polyoxyl 40 Hydrogenated Castor Oil as an edge activator, substantially lower values of ZP were obtained, in contrast to those obtained using a lower amount of surfactant. This outcome may be due to the hydrophilic nature of Polyoxyl 40 Hydrogenated Castor Oil, which enables it to remain on the surface of transferosomes and mask charge.[104] The branched structure of Polyoxyl 40 Hydrogenated Castor Oil probably prevents the appropriate accumulation of its molecules by creating closed vesicular structures owing to the developed steric barrier.[105] The nasal mucosa showed a weak negative potential. Consequently, the negative surface charge of optimized transferosomes may improve drug permeation through the nasal mucosa owing to electrostatic repulsion.[106]

Selection of Optimized Transferosomes Formulation

The desirability measures via graphical and numerical optimization methods were the basis for choosing the optimal formula. The selected criteria for each response determine various desirability functions. The detected response can be transformed into a desirability value by using the desirability approach. This value increased as the corresponding response value approached its optimum value. The desirability value is between 0 and 1. The ideal formula has a desirability value of 1, whereas the worst possible formula has a desirability value of 0. The formulation with the highest desirability value was selected as the optimal formulation.[107] Based on the polynomial formulae (1–4), an optimization study was carried out to obtain A, B, and C levels that would reduce vesicle size, ZP, and PDI while magnifying EE% for imperative vesicle efficiency. The optimized formulation composed of Phospholipon® 90G: 100 mg, Polyoxyl 40 Hydrogenated Castor Oil: 30 mg in chloroform/methanol (2:1 v/v, 30 mL), the produced film hydrated with SNF (pH 5.5, 10 mL including 30 mg Transcutol), showed particle size of 664.3 ± 69.3 nm, encapsulation efficiency (EE%) of 82.8 ± 0.02%, surface potential of −11.23 ± 2.5 mV and PDI of 0.6 ± 0.03 (Table 2). The design validity was demonstrated by the agreement between the experimental values for the best formula responses and the estimated values computed using the software.

Visual Appearance, Clarity, pH, Gelation Temperature ($T_{sol\text{-}Gel}$), Viscosity, and Mucoadhesion of the Developed in-situ Gels

The delivery of drugs in the form of in situ gel provides many advantages because before its nasal administration, its fluid-like state makes it simple to instill as a droplet, enabling precise dosage, but hardened into a gel with an extended residential period at the temperature of the body.[57]

All prepared curcumin transferosome in situ gels were clear, yellow, and transparent, without impurities or turbidity. The pH of in situ gels ranges from 4.4 to 5.3, making them acceptable for nasal administration[48] (Table 3). The drug content ranged from 96.018 ± 6.8 to 98.495 ± 0.5%, indicating a uniform distribution of curcumin transferosomes in the in-situ forming gels, Table 3. The gelation temperature varied from 33 ± 1.0 °C to 53.35 ± 1.5 °C, Table 3. The gelling temperature is one of the main decisive factors in the in situ gel formulae. The characteristics of the nasal cavity define the properties needed for the mucoadhesive nasal gel, such as gelation temperature, which should be between 32 °C and 34 °C, and a short duration of gelation to permit adhesion to the mucosal membrane and stop rapid drainage of the preparation.[108,109] Because of its reduced critical solution temperature, Poloxamer 407 has thermoreversible attributes. At body temperature, it undergoes a sol-gel shift and forms an in situ gel.[42] Carbopol is a mucoadhesive polymer that is capable of enhancing the bioavailability of intranasally administered therapeutics and improving their stability by inhibiting proteolytic enzymes.[110,111] Previously, it was noted that $T_{sol\text{-}gel}$ was higher than 40 °C when Poloxamer 407 was employed solely to form in-situ gelling preparations at 15% w/w

Table 3 Composition and Evaluation of Different Pluronic®-Based Intranasal in-situ Gelling Formulations (Means ± SD, n = 3)

Formula Code	Composition (% w/v)			Clarity			pH			Gelling Temp °C	Drug Content (%)	Viscosity (mPa, 30 rpm)			Muco-adhesive Force (Pa)
	Cp 934	Poloxamer 407	Poloxamer 188	4°C	25°C	Gelling Temp	4°C	25°C	Gelling Temp			4°C	25°C	Gelling Temp	
F1	0.25	16	5	Clear pale yellow	Clear pale yellow	Clear pale yellow	4.4 ± 0.14	4.37 ± 0.1	4.35 ± 0.03	53.35 ± 1.5	97.966 ± 2.249	350 ± 50	1600 ± 174.36	3000.67 ± 57.7	2.1 ± 0.37
F2	0.125	16	10	Clear pale yellow	Clear pale yellow	Clear pale yellow	4.65 ± 0.06	4.58 ± 0.06	4.59 ± 0.09	41.33 ± 1.12	97.317 ± 4.902	488.67 ± 138.9	2666.67 ± 472.6	3600 ± 100	2.2 ± 0.11
F3	0.025	16	15	Clear pale yellow	Clear pale yellow	Clear pale yellow	5.3 ± 0.015	5.3 ± 0.01	5.2 ± 0.17	53.33 ± 1.52	97.052 ± 1.322	727.67 ± 342.7	3233.33 ± 493.3	4566 ± 288.68	3.62 ± 0.03
F4	0.25	20	5	Clear pale yellow	Clear pale yellow	Clear pale yellow	4.48 ± 0.015	4.72 ± 0.4	4.9 ± 0.3	35.66 ± 0.58	97.7496 ± 0.992	295.33 ± 97.11	1000 ± 317.22	4900 ± 200	4.34 ± 0.05
F5	0.125	20	10	Clear pale yellow	Clear pale yellow	Clear pale yellow	4.58 ± 0.012	4.6 ± 0.1	4.72 ± 0.12	36.66 ± 0.57	96.018 ± 6.840	420 ± 58.59	1643.33 ± 193	5200 ± 493.28	4.96 ± 0.1
F6	0.025	20	15	Clear pale yellow	Clear pale yellow	Clear pale yellow	5.3 ± 0.15	5.12 ± 0.23	5.6 ± 0.08	36.66 ± 0.6	97.341 ± 1.499	683.33 ± 115.5	1900 ± 173.21	7200 ± 160.72	8.3 ± 1.15
F7	1	20	20	Clear pale yellow	Clear pale yellow	Clear pale yellow	5.3 ± 0.1	5.32 ± 0.08	5.3 ± 0.03	33 ± 1.0	98.495 ± 0.499	783.33 ± 28.87	3833.33 ± 321.46	8700 ± 305.5	11.00 ± 0.05

https://doi.org/10.2147/IJN.S423251

concentration, which is unfavorable for intranasal in-situ gelled formulations. To modify the temperature of the phase transformation to be in the appropriate temperature range (~ 32–34 °C), two approaches were used: varying concentrations of Poloxamer 407 and mixing blends of Poloxamer 407 with other polymers (Poloxamer 188 and CP934). The combination of Poloxamer 407 with other polymers is also beneficial for slowing down its relatively quick dissolution under physiological conditions.[51,52] Table 3 demonstrates an inverse relationship between $T_{sol\text{-}gel}$ and the Poloxamer 407 concentrations. As illustrated, $T_{sol\text{-}gel}$ decreased from > 40 to 33 ± 1.0 °C as the polymer concentration increased from 16 to 20% w/w. This result is in line with prior investigations.[54,112] This is most likely explained by the easy entanglement and packing of Poloxamer micelles at increased concentrations, which induces gel formation at a reduced temperature.[113,114]

To modify the gel properties and gelling temperature, Poloxamer 407 was incorporated into the Poloxamer 188. Polymeric systems of Poloxamer 407 at 16% and Poloxamer 188 at 5, 10, or 15% led to a $T_{sol\text{-}gel}$ more than 40 °C (Table 3). The inclusion of 15% or 20% of Poloxamer 188 to 20% of Poloxamer 407 led to a $T_{sol\text{-}gel}$ of 36.66 ± 0.6 °C and 33 ± 1.0 °C, respectively. Poloxamer is a triblock copolymer (PEO-PPO-PEO) composed of 70% hydrophilic polyoxyethylene (PEO) and approximately 30% lipophilic polyoxypropylene components (PPO),[115,116] which $T_{sol\text{-}gel}$ is governed by the polymer molecular weight and ratio of PEO/PPO. $T_{sol\text{-}gel}$ decreased with increasing molecular weight, whereas $T_{sol\text{-}gel}$ increased with an increasing PEO/PPO ratio.[117] The dehydration of the hydrophobic PPO unit of Poloxamer 407 controls the gelling mechanism, resulting in the generation of micelles at the critical temperature. Poloxamer 188, which contains approximately 16% PPO and 84% PEO, will lower the PPO to PEO ratio, resulting in intermolecular hydrogen bonding and rising in $T_{sol\text{-}gel}$.[115] Poloxamer 188 has a higher PEO/PPO ratio than Poloxamer 407, which causes $T_{sol\text{-}gel}$ for mixtures of Poloxamer 407 and Poloxamer 188 to increase up to a particular concentration. Above this concentration, the solution $T_{sol\text{-}gel}$ dropped with an additional increase in the amount of Poloxamer 188. These outcomes are consistent with earlier reports.[52,118] The viscosity values were in the range of (295.33 ± 97.11 to 783.33 ± 28.87 mPa, at; 4 °C, 30 rpm). There was a marked rise in the viscosity of gel preparations when measured at their respective gelling temperatures (3000.67 ± 57.7–8700 ± 305.5 mPa, 30 rpm) (Table 3). At low temperatures, hydration of the polymeric molecules occurs and the interactions between them are limited to simple entanglement. When the temperature was increased, dehydration of the polymer molecules occurred gradually until complete dehydration occurred. An experimentally observed sharp increase in viscosity at high temperatures indicates that associations between polymers occur and the system approaches an infinite network configuration.[67]

Mucoadhesion is an influential physicochemical factor for in situ nasal gels because it prevents fast drainage and prolongs the residence duration.[119] The alteration in mucin viscosity upon incorporation into the in situ gel preparations was detected and used as an indication of the magnitude of mucoadhesive characteristics. The increase in the polymer concentration improved the mucoadhesion of the gels owing to the interaction of Carbopol with mucin via hydrogen bonding.[67] The high mucoadhesive effect and viscosity of curcumin gel are anticipated to extend its nasal retention and improve its permeation and therapeutic activity.[34]

Rheological Studies

The rheological behaviors of the gels formed in situ at 4 °C and 25 °C, and the gelling temperature are shown in Figure 5A-C. The prepared gels displayed the criteria of a pseudoplastic system (shear-thinning effect) at the studied temperatures, where increasing the shear led to reduced viscosity. The systems had a low viscosity in their liquid state before gelation, which was slightly altered as the shear rate increased. A desirable nasal in situ gel formula should have reduced viscosity when applied to the nose, becoming adequately viscous after administration to be retained at site.[120] As the temperature increased, the viscosity of the preparations also increased. The Shear-thinning behavior was noticeable, and the viscosity significantly increased as the temperature increased from 4 °C to the gelling temperature. Increasing the viscosity resulted in a shift from liquid to gel to a specified degree inside the nose. In addition, the gels encountered a decrease in their viscosities with increasing shear rate, supporting the pseudoplastic effect.[57] In contrast to a high-viscosity Newtonian fluid, the pseudoplastic criterion enables a sustained drug release and satisfactory gel distribution over the nasal surface.[121,122]

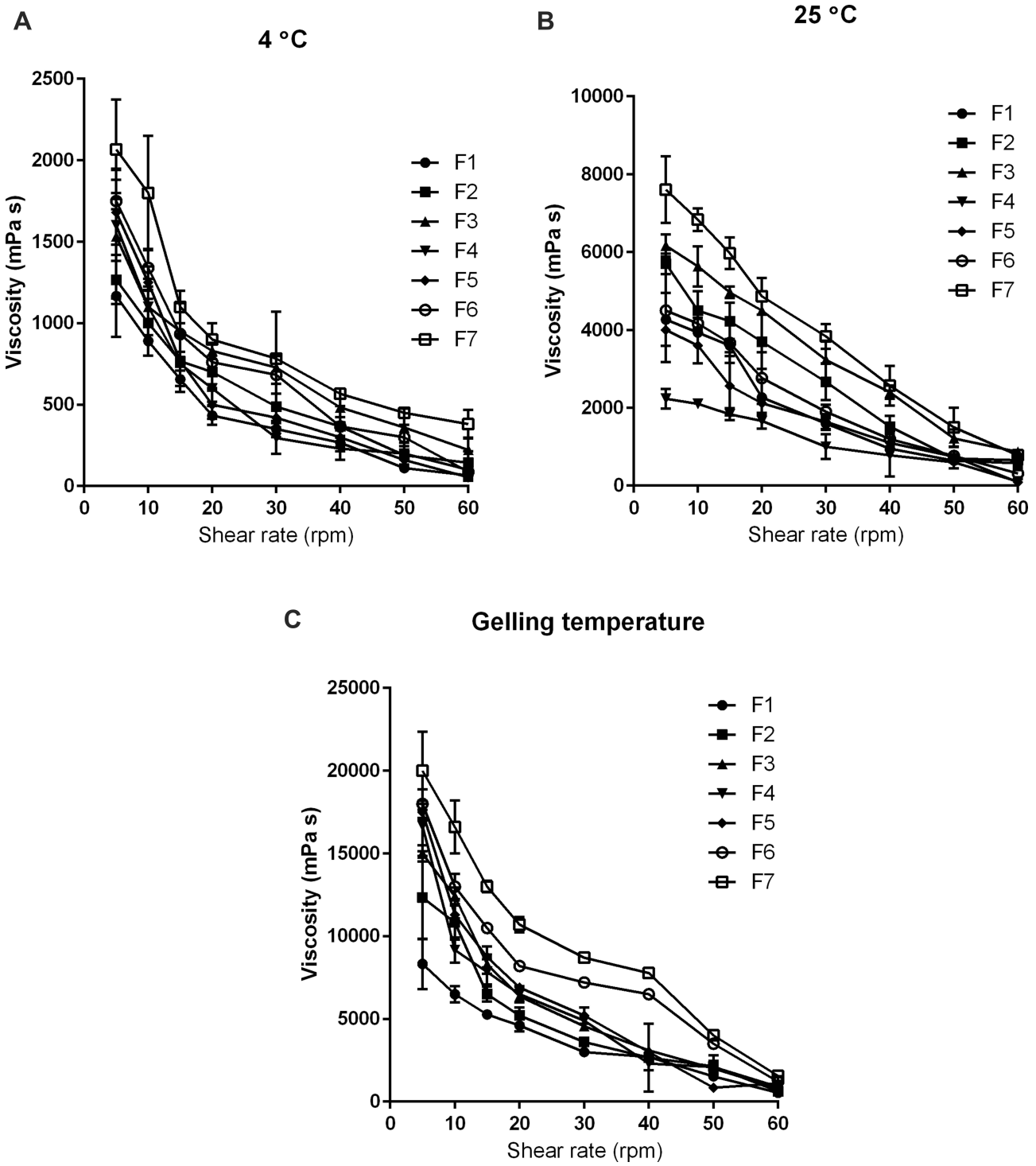

Figure 5 Rheological profiles of in-situ gel formulations. (**A**) at 4 °C, (**B**) at 25 °C, and (**C**) at gelling temperature.

Fourier Transform-Infrared (FT-IR) Spectroscopy

Curcumin powder (Figure 6A) displayed distinctive bands at 3508 cm^{-1} attributed to phenolic O-H moiety stretches, 1628 cm^{-1} due to aromatic C=C stretching), and benzene ring stretching bands were observed; at 1597 cm^{-1}, vibrations of C=O and C=C groups were observed at 1509 cm^{-1}, bending bands of olefinic C-H group were recorded at 1428 cm^{-1}, and aromatic (C–O, C–O–C, Benzoate trans-CH, and benzoate cis-CH) moieties were observed at 1278 cm^{-1}, 1024 cm^{-1},

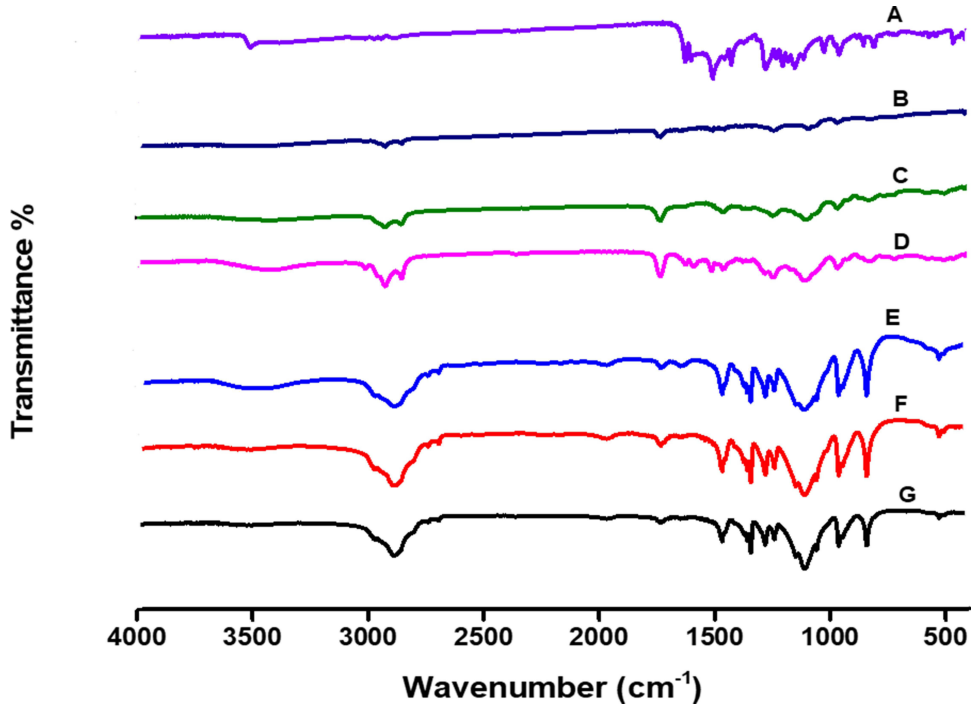

Figure 6 FTIR spectra of (**A**); Curcumin powder, (**B**) Physical mixture (Phospholipon® 90G + Polyoxyl 40 Hydrogenated Castor Oil + curcumin), (**C**) Plain freeze-dried transferosomes, (**D**) Curcumin transferosomes freeze-dried powder, (**E**) Freeze dried free curcumin gel, (**F**) Freeze dried plain gel, and (**G**) Freeze dried curcumin transferosomes gel. (**E-G**) show similar absorption bands because all of them share the same composition of gel (Poloxamer 407 and Poloxamer 188, and CP 934P). The absence of characteristic bands of curcumin in the free drug loaded gel formulation (**E**) may indicate drug-polymer molecular interactions and solid solution formation of curcumin in the polymeric network of the gel. Besides, the disappearance of all the distinguishing bands of curcumin in the freeze-dried curcumin transferosome-loaded gel formulation (**G**) may be explained by drug dissolution in lipids and encapsulation within the transferosome-loaded gel.

959 cm^{-1}, and 713 cm^{-1}, respectively.[123,124] The IR spectrum of the physical mixture (Phospholipon® 90G + Polyoxyl 40 Hydrogenated Castor Oil + curcumin) (Figure 6B) revealed the disappearance of distinctive bands of curcumin; the disappearance of distinct absorption bands of phospholipids corresponding to C–H group stretching at 2926 and 2855 cm^{-1}; and a reduction in the carbonyl group stretching, water scissoring, and PO_4 stretching bands at 1737 cm^{-1}, 1648 cm^{-1}, and 1249 cm^{-1}, respectively.[125] In addition, the disappearance of the characteristic bands of Polyoxyl 40 Hydrogenated Castor Oil corresponding to the hydroxyl moiety at 3386 cm^{-1} and reduction in the bi-forked peak at 2856 and 2904 cm–1[77] indicate that the drug and formulation ingredients interact chemically. The peak locations of the plain transferosome preparations (Figure 6C) appeared at wave numbers identical to those of its constituents (Phospholipon® 90G and Polyoxyl 40 Hydrogenated Castor Oil). Freeze-dried curcumin transferosome powder (Figure 6D) exhibited peaks for Polyoxyl 40 Hydrogenated Castor Oil and Phospholipon® 90G. The disappearance of the phenolic hydroxyl band of curcumin in the transferosome formulation suggests that phospholipids and curcumin interact via hydrogen bonding. Moreover, a reduction in other characteristic curcumin bands confirmed the loading of curcumin within transferosomes. The FTIR spectrum of the freeze-dried free curcumin gel (Figure 6E) revealed specific bands of Poloxamer 407 and Poloxamer 188 at ~3453 cm^{-1}, 2886 cm^{-1}, and 1113 cm^{-1} related to O–H, C–H, and C–O stretching groups, respectively, which are in agreement with published values.[113] Additionally, CP 934P characteristic hydroxyl and carboxyl group bands were present at 2926.87 cm^{-1} and 1644.84 cm^{-1}, respectively.[126] The absence of curcumin bands in the free drug-loaded gel formulation may indicate drug-polymer molecular interactions and solid solution formation of curcumin in the polymeric network of the gel.[127] The freeze-dried plain gel (Figure 6F) showed bands characteristic of poloxamers and CP 934P. The disappearance of all the distinguishing bands of curcumin in the freeze-dried curcumin transferosome-loaded gel (Figure 6G) favored drug dissolution in lipids and encapsulation within the transferosome-loaded gel. Differential scanning calorimetry (DSC) studies were performed to confirm these findings.

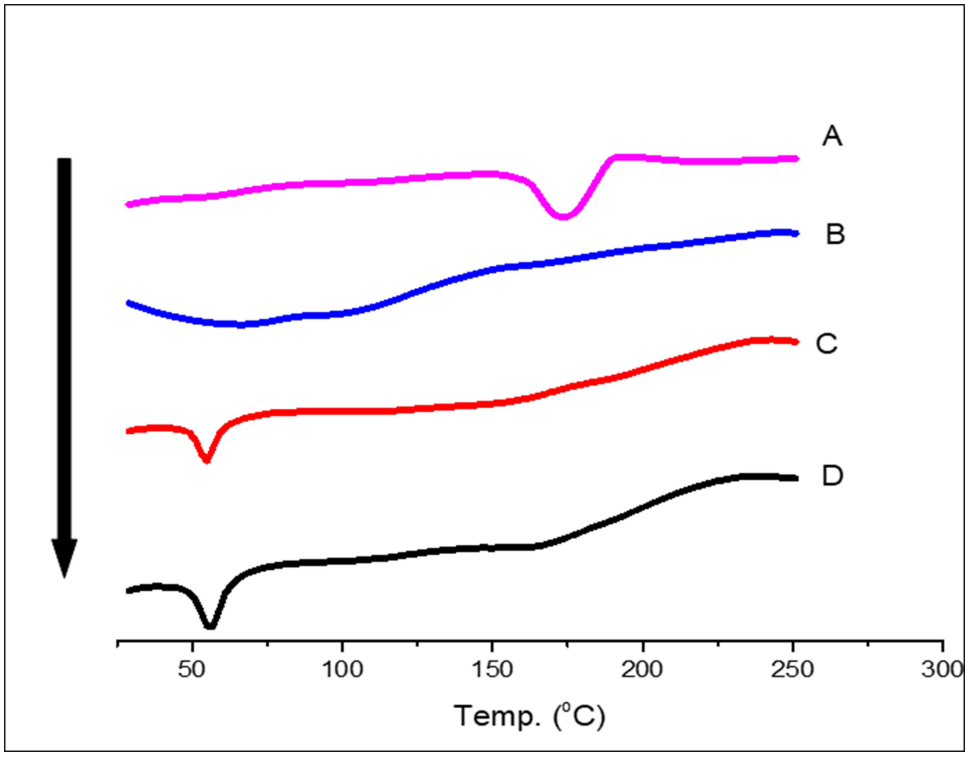

Figure 7 DSC thermogram of (**A**); Curcumin powder, (**B**) Freeze dried free curcumin gel, (**C**) Freeze dried plain gel, and (**D**) Freeze dried curcumin transferosomes gel.

DSC Analysis

DSC analysis is beneficial for investigating mixture behaviors and drug-lipid interactions. DSC thermogram of curcumin is presented in Figure 7A, showing a sharp endothermic peak at 173 °C associated with a melting degree.[128] The vanishing of the curcumin peak in the thermogram of the free curcumin gel formula indicates the drug solubilization and its presence in either an amorphous or molecularly dispersed formation upon incorporation into the gel structure,[111] Figure 7B. DSC thermograph of freeze-dried plain gel and drug-loaded transferosomal gel (Figure 7C and D) displays a sharpened endothermic curve beginning at 52.12 °C, reflecting the melting transition of poloxamer 407 and poloxamer 188 surfactants.[129] However, this peak was not observed in the thermogram of free curcumin-loaded gel. Moreover, amorphization of the drug and perfect encapsulation within the lipid matrix of transferosomes resulted in the disappearance of the drug peak in the curcumin transferosome gel formulation Figure 7D. This observation is consistent with earlier studies that reported identical behaviors of drug-loaded vesicles in gel formulations[76,130] where the characteristic peaks of the tested drug products were vanished completely from the thermograms of drug loaded vesicles, indicating drug solubilization in the lipid phase and existence in amorphous state hence, the efficiency and success of the hydrophobic drug encapsulation within lipid matrix of the vesicles.

In vitro Curcumin Release

The percentage drug released from the developed transferosomal gel formula was estimated in SNF (pH 5.5, 5% Tween 80 at 37 ± 0.5 ˚C), utilizing the dialysis membrane diffusion method. The release pattern of curcumin from the transferosomal gel formula compared with the free curcumin-loaded in situ gel formula, curcumin-loaded transferosomal dispersion, and free curcumin dispersion is displayed in Figure 8A. The curcumin-loaded transferosomal suspension showed an early drug diffusion of 0.819 ± 0.002% in the first 6 h, followed by extended drug release (9.512 ± 0.008%) for more than 48 h. While; the Curcumin dispersion showed a maximum drug release of 3.222 ± 0.002% over 48 h. Drug release from the curcumin dispersion was low because of its reduced aqueous solubility (11 ng/mL).[131] The higher in vitro release percentage of curcumin from transferosomal dispersion versus free drug dispersion is ascribed to the

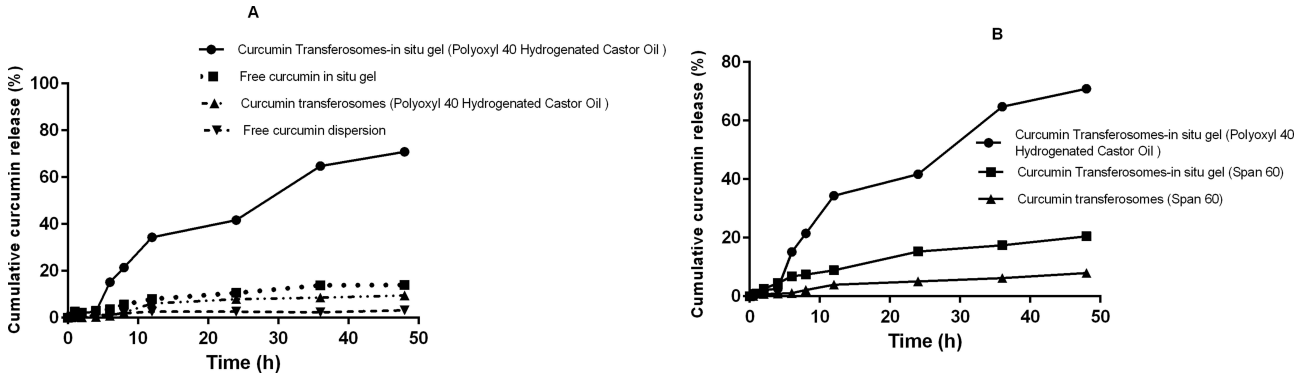

Figure 8 (**A**) Cumulative in vitro release patterns of curcumin from in-situ gel (F7), curcumin suspension, transferosomes dispersion (Polyoxyl 40 Hydrogenated Castor Oil), and transferosomes- in-situ gel (Polyoxyl 40 Hydrogenated Castor Oil) formulations in artificial nasal fluid (SNF, pH 5.5, 5% tween 80) at 37 °C. (**B**) Cumulative in vitro release profiles of curcumin transferosomes dispersion (Span 60), and curcumin transferosomes- in-situ gel (Span 60) compared with curcumin transferosomes- in-situ gel (Polyoxyl 40 Hydrogenated Castor Oil) formulation in artificial nasal fluid (SNF, pH 5.5, 5% tween 80) at 37 °C. Data are represented as mean ± SD (n= 3).

double impact of permeation enhancers (Transcutol® P) and Polyoxyl 40 Hydrogenated Castor Oil surfactant, as they enhance the partitioning of curcumin from the transferosomal formulation by enhancing the vesicular bilayer fluidity and boosting the solubility of curcumin.[108,132] Free drug-entrapped in-situ gel preparation yielded a drug release of 3.631 ± 0.002% in 6 h. Subsequently, 14.028 ± 0.006% maximum drug release was recorded from the gel during 48 h. Water diffusion into the in-situ gelling systems and drug distribution through the swollen matrix are essential for drug release from gel preparations.[41] The total load released from curcumin transferosome gel was 15.175 ± 0.008% over 6 h, accompanied by a considerably slow extended release of 70.868 ± 0.001% over 48 h. As indicated by the inflection points of the release profile, drug release was initially quick because the gel had not fully formed. Later, slower drug release from the in situ gel occurred because of gelation.[133] The recorded results were primarily attributed to the gelling effects of CP 934P, P 407, and P188, which are responsible for controlling curcumin release.[37] From nano-transferosomes, Enhanced drug absorption was observed because of the reduced particle size. The enhanced drug release from the transferosome-laden in situ gel in comparison with transferosome dispersion and free drug-loaded gel might be ascribed to the drug existence in nanolipid vesicles. Moreover, the inclusion of molecules of surface-active agents in these vesicles (Polyoxyl 40 Hydrogenated Castor Oil) will augment drug partitioning from the vesicular delivery system as the surfactants become connected to the phospholipid bilayer, thereby increasing drug release from the vesicles.[134] In addition, high edge activator levels could enhance the fluidity of the phospholipon® 90G double layer, which would increase the permeability of the vesicular membrane and, thus, increase the drug release rate.[135] Based on a previously published study, encapsulating water-insoluble medications in transferosomes increased their dissolution rate.[136] Additionally, PF68 is an amphiphilic copolymer that functions as a pore-forming and release-enhancing agent, while PF127 acts as a gelling agent and solubilizer of poorly soluble drugs.[137]

A comparison of the in vitro release profiles of transferosome gels prepared using Polyoxyl 40 Hydrogenated Castor Oil and Span 60 surfactants revealed an extremely significant variation ($p < 0.0001$) in the curcumin release percentage after 6 and 48 h (Figure 8B). The percent curcumin release from Span 60- based transferosomes gels was 20.509 ± 0.005% at the end of the 48-h experiment. This observation may be explained by the superior solubilization ability of Polyoxyl 40 Hydrogenated Castor Oil.[81] Mazyed et al[77] made the same assessment and noted an improved acetazolamide release from transferosomes composed of Polyoxyl 40 Hydrogenated Castor Oil. These results were attributed to the softening and deformation of the vesicle membrane owing to the edge activating and bilayer softening characteristics of Polyoxyl 40 Hydrogenated Castor Oil.[138] In addition, hydrophilic vesicles constantly attempt to prevent dehydration by migrating to layers abundant in water, which is considered a transport approach connected to the osmotic gradient.[139]

Kinetic data were analyzed by fitting different mathematical models to distinguish the mechanisms that simulate drug release from various preparations.[65] The outcomes are outlined in Table S2. The best fit model for curcumin release from the in situ gel, transferosome dispersion, and drug dispersion preparation was the Higuchi diffusion mechanism. This result demonstrated a diffusion-based curcumin permeation mechanism. In addition, the Korsmeyer-Peppas model was

used as a semi-empirical equation to analyze the results and understand drug release kinetics. The calculated n value was in the range of 0.5–1 for the in vitro release results of free drug incorporated in-situ gel, indicating an anomalous non-Fickian transport, where the curcumin release is controlled by swelling and diffusion of curcumin via the channels of water across the gel matrix.[140] This finding demonstrates that gel dissolution controls drug release.[48] For drug dispersion, the n value was ~ 0.5, which corresponds to the Fickian mechanism, where curcumin release is controlled by diffusion. For the transferosome suspension, the calculated n value was found 1.09 ± 0.194 which suggests that drug release from this system obeyed the non-Fickian (super case-II) transport path.[106] This result may confirm that the release of curcumin from transferosomes vesicles is governed by coupling of diffusion mechanism from the lipid vesicles and by erosion of the compact phospholipid bilayer. On the other hand, the best-fit model for curcumin release from transferosome-loaded in situ gel formula was the first-order model, and the n value was 1.182 ± 0.148 which indicated the reliance of drug release from transferosomes on the concentration gradient in the diffusion cell. This case II transport also confirms that the drug release from transferosome-loaded in situ gel is controlled by diffusion mechanism through gel matrix and the rate of gel network swelling. Thus, based on these results, it can be concluded that utilizing of transferosomes vesicles of curcumin provides potential reservoir systems for continuous delivery of the encapsulated drug in both transferosome suspension and transferosomes in situ gel formulations. This result was in line with earlier studies that clarified the same release patterns of transferosomes in situ gels.[141]

Morphology

The surface characteristics of the fabricated curcumin-loaded transferosome dispersion and the curcumin-loaded transferosomes incorporated into the in situ gel were compared using SEM (Figure 9A and B). Vesicles of transferosomes emerged as a uniform dispersion of distinctive, nearly spherical particulates with smooth surfaces and loose aggregates (Figure 9A). In addition, the estimated size agreed with that obtained by DLS (Table 2). Morphological investigation of curcumin transferosome-loaded in situ gel formulation (Figure 9B) verified that the transferosome vesicles maintained their spherical form after embedding within the in situ gel matrix.[142]

Ex vivo Permeability Evaluation

The nasal mucosa of sheep was used as an in vitro test to compare the intranasal permeability characteristics of curcumin transferosomes incorporated in an in situ gel versus free curcumin in situ gel to gain knowledge of the in vivo efficacy of the optimum curcumin transferosome-loaded in situ gel. The cumulative percentage of curcumin transported from the transferosome-loaded in situ gel, as opposed to the free drug-loaded in situ gel, is illustrated in Figure 10. The optimized curcumin transferosome-incorporated in-situ gel displayed a significant enhancement in the percentage of cumulative drug permeated versus free drug gel ($p < 0.0001$), with 25.044 ± 1.579% permeation of drug after 6 h, in comparison to only 4.771 ± 0.469% curcumin transport from the free curcumin loaded gel at the exact period. The highest percentage of curcumin diffused after 24 h from the selected curcumin transferosome-loaded in situ gel was approximately 2.58-times larger than that of the free curcumin gel. As displayed in Figure S1, large portions of curcumin diffused from the

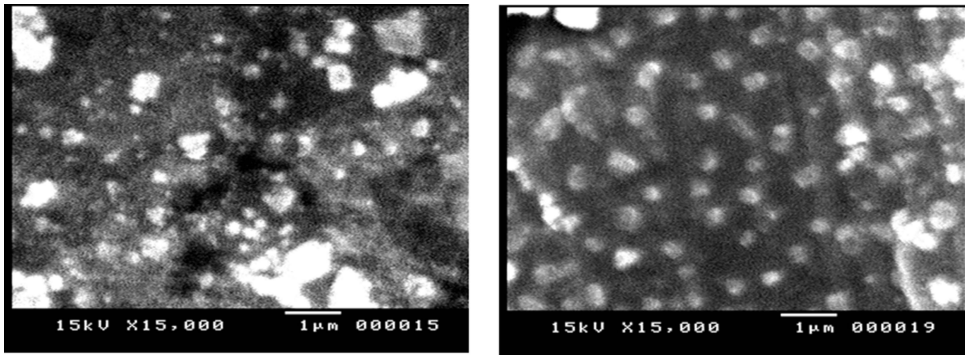

Figure 9 Representation showing SEM micrographs of curcumin-loaded transferosomes ((**A**), × 15,000) and curcumin transferosomes loaded in-situ gel ((**B**), × 15,000).

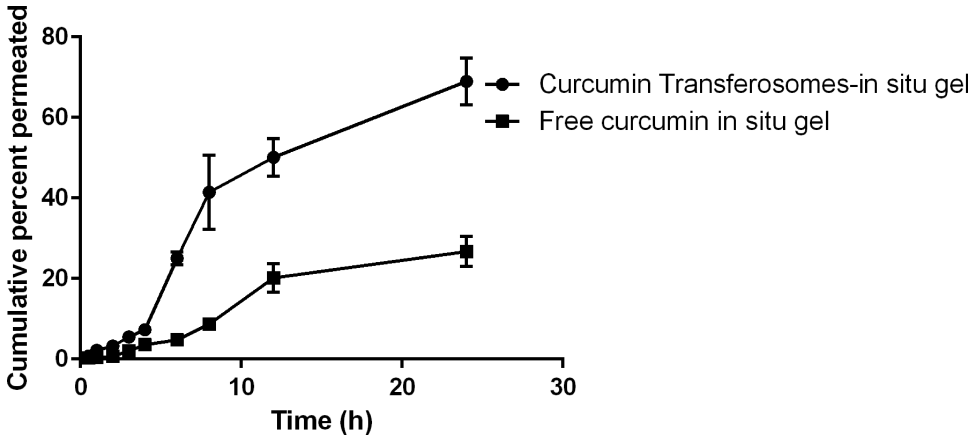

Figure 10 Profile of ex vivo transport of the optimum curcumin transferosomes-loaded intranasal in-situ gel in comparison to free curcumin in-situ gel in SNF, pH 5.5, 5% tween 80 at 37 °C (findings displayed as average ± SD, n = 3).

prepared transferosome-loaded in-situ gel formulation across nasal mucosa after 24 h incubation (68.96 ± 5.8%), which could be adequate for its therapeutic potential. The coefficient of apparent permeability (P_{app}) computed for free curcumin gel diffusion across the nasal membrane was 1.099 ± 0.161×10^{-6} cm/s. The transfer rate of curcumin when enclosed as transferosomes within the thermosensitive in situ gel was increased by approximately three times, according to the value of P_{app} computed from the linear flux of curcumin- nano transferosomes in situ gel through nasal tissue (2.834 ± 0.137×10^{-6} cm/s) (Table 4). Furthermore, compared with the steady-state flux of curcumin added to the donor cell as a free drug gel, the quantitative mass transfer of curcumin through the nasal mucosa was significantly elevated when applied as curcumin transferosomes within in situ gel (Table 4). The enhanced permeation of curcumin from the optimized transferosomal gel may be due to the synergistic advantages of transferosome vesicles with nanosized diameters and the unique properties of the Pluronic-based gel.[136] The deformable and elastic structures of transferosomes may have the potential to press themselves into the deeper biological membrane layers. Additionally, the inclusion of surfactants, which act as edge-activating agents, may contribute to the permeability of transferosomes by fluidizing or rupturing the membrane lipid bilayer.[136] Phospholipones are strongly attracted to biomembranes, increasing the penetration efficiency of transferosomes.[77] In addition, the nanoscale diameter of transferosomes leads to a large surface area, extending the contact zone with the mucosal membrane and subsequently increasing the possibility of curcumin penetration.[45] In addition, transferosomes improve the solubility of insoluble therapeutics in biological media. According to previous studies, nanovesicles can increase drug absorption across the nasal barrier and significantly increase the bioavailability of therapeutics.[143] However, the interaction period of the drug-encapsulated transferosomes on the nasal mucosal surface may have been shortened by mucociliary clearance. Thus, the use of thermosensitive in situ gels with particular properties, such as thermoreversible gelation and micellar characteristics, has recently been investigated as a beneficial platform for preparing stabilized nanoscopic vehicles for smart drug delivery. The slight disordering of biological membranes caused by the pluronic-based gel could enhance drug transport by diffusion across the lipid intracellular matrix.[144] The gel has an occlusive property that makes it easier for the skin to hold onto water,

Table 4 Permeation Properties Across Nasal Mucosa

Formulation	*Papp (× 10^{-6}) cm/s*	*Jss (μg cm^{-2} h^{-1})*	*ER* [a]
Curcumin transferosomes in-situ gel	2.834 ± 0.137***	5.102 ± 0.247***	2.58
Free curcumin in-situ gel	1.099 ± 0.161	1.979 ± 0.289	——

Notes: Each value is expressed as mean ± SD (n = 3). ***Extremely significant different from free curcumin in-situ gel ($p < 0.001$). [a]The enhancement ratio (ER) was computed as $P_{app\ (curcumin\ transferosomes\ in\text{-}situ\ gel\ formulation)}/P_{app\ (free\ curcumin\ in\text{-}situ\ gel)}$.

Abbreviations: J_{ss}, steady-state flux; ER, enhancement ratio.

increasing its hydration for a longer times.[145] Moreover, transferosomes within the gel network may enhance the mechanical strength and offer remote-controlled applications.[146,147]

Suitable kinetic models were applied to compare the transport mechanism of curcumin transferosomes in situ-forming gels and the free curcumin-incorporated in situ gel through the nasal mucosa (Table S3). The findings showed that ex vivo curcumin diffusion from transferosomal in situ gel preparations across the nasal membrane followed the Korsmeyer-Peppas model and that free curcumin in situ gel followed the first-order model. The estimated diffusion exponent (n) values were 1.249 ± 0.046 and 1.355 ± 0.066 for the curcumin transferosomal in situ gel and free curcumin in situ gel, respectively, suggesting that drug transport from these in situ gels matched the case-II transport path. Case -II transport path means that the drug permeation pattern from both formulations is controlled by diffusion mechanism through lipid vesicle or gel matrix and by erosion of the gelling polymer. Similar results have already been documented.[106,148]

Stability Assessment

The optimized transferosomes were kept at 4.0 °C and 25 °C to examine their stability (Table S4). Vesicle size, surface charge, PDI, and encapsulation efficiency were assessed over 2 months. At the specified storage temperature, no sedimentation, aggregation, or fusion of vesicles were observed ($P > 0.05$). However, transferosomes displayed a slight decline in encapsulation efficiency percent ($p < 0.05$) after one month and a very significant decline ($p < 0.01$) after two months at 4.0 °C. When kept at room temperature, the change in encapsulation efficiency percentage was very significant ($p < 0.01$) after 30 days and extremely significant ($p < 0.001$) after 60 days, although the variation was only about ~ 6%. This result could be ascribed to drug leaching from the developed transferosomes, which might be due to the chemical deterioration of phospholipids, which disrupted the membrane arrangement and resulted in drug leakage depending on the storage temperature.[134,149] Variations in clarity, pH, drug content, viscosity, and mucoadhesion force for the optimized curcumin transferosomal in situ gel (F7) were monitored over 60 days (Table S5). No noticeable variations were recorded in the evaluated criteria, as estimated by one-way ANOVA and Student's *t*-test, except for some changes in the viscosity and mucoadhesive force. A significant decline in the viscosity of F7 was observed after 1 month ($p < 0.05$) and after 60 days ($p < 0.01$) at 40°C. Moreover, a slight decrease in mucoadhesive force was recorded after 60 days at 4 °C ($p < 0.05$) and at 25 °C ($p < 0.01$) but remained within appropriate limits. It could be deduced from the stability data that maintaining transferosome-loaded in situ gel formulation at 4 °C is the ideal way to reduce any instability problems. Similar results were previously recorded.[37,108,142]

Antiviral Effect

In line with the infinite research efforts since its sudden emergence, this study proposed the potential of the curcumin nanosystem to inhibit SARS-CoV-2 propagation via interaction with the spike glycoprotein and blocking ACE2 enzyme, viral protease, or RdRp enzymes, as speculated by molecular docking studies. In this context, a cell-based cytopathic effect (CPE) test of the SARS-CoV2 virus in Vero E6 cell lines was employed to test the potency of the developed curcumin transferosomes loaded in situ-forming gel for anti-SARS-CoV2 activity. The MTT test was employed to estimate the CC50 of the tested compound to rule out any potential cytotoxicity or anti-cell proliferation influence of the tested formulation on the subjected cells.[23,150,151] The dose–response determined by staining with crystal violet was used to detect the antiviral activity.[152] The MTT assay and results of antiviral activity are graphically represented in Figure 11. It was depicted the curcumin transferosomes in-situ gel formulation was capable of inhibiting SARS-CoV-2-induced CPE by 50% at a concentration of 7.018 µg/mL, the CC50 was equal to 1150 µg/mL. These findings prove that the developed curcumin formulation has strong antiviral potential at low concentrations. In addition, a reduced cytotoxic effect was noted, primarily attributed to the existence of transferosomes within the in situ gel formulation, thus preventing the drug from directly acting on cells.[153] These results confirmed the in silico analysis and demonstrated the role of curcumin nanovesicles in the inhibition of both viral entry and replication.

The advanced antiviral effect could be attributed to the probable interaction of the developed transferosomes with virus-infected cells via either fusion or endocytosis.[154] The focused augmented activity of the produced formulation at the cellular interface, as an outcome of transferosomal gel adherence onto the membrane surface, leads to greater transport of hydrophobic therapeutics.[155] In addition, the edge activators incorporated in the preparation of the

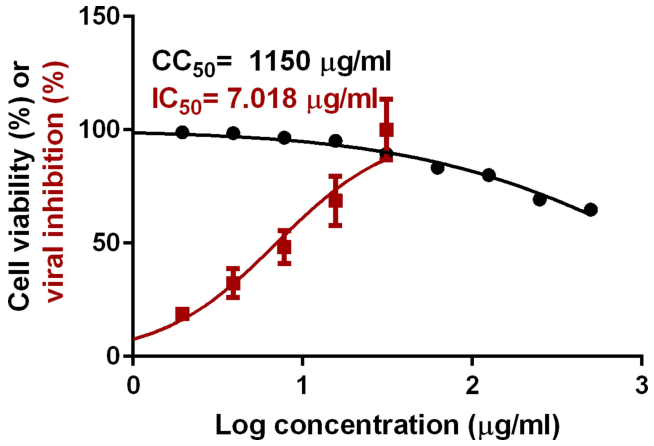

Figure 11 % Cell viability and % viral inhibition of the investigated curcumin transferosomes in-situ gel at various concentrations in Vero-E6 cells and represented as % cell viability or % viral inhibition versus log_{10} concentrations. The test sample expressed an enhanced antiviral efficacy against SARS-CoV-2.

transferosomal gel play a decisive role in promoting the permeability of curcumin through virus-infected cells.[156,157] These findings are in agreement with those of a previous investigational study that documented the impact of vesicular delivery systems on boosting curcumin antiviral activity versus HSV.[158] Moreover, The selectivity index (SI) was calculated by dividing the level of (50% cellular cytotoxicity) by (the 50% effective level), which compares a compound's effectiveness in preventing viral replication with its cytotoxic action.[159] Generally, a high selectivity index signifies augmented therapeutic activity of the formulation. Interestingly, the SI value of the developed curcumin transferosome in situ gel formulation was (163.9), indicating enhanced selectivity of the formula.

Recently, Mahmoud et al[160] compared the antiviral potential of various edge activator-based nanostructures of curcumin with a surfactant-free formulation against SARS-CoV-2. The values of the obtained selectivity indices of the different formulations were much lower than those of our transferosomal in situ gel formulation, indicating the high therapeutic activity of the developed preparation. Earlier investigations have illustrated the inhibitory efficacy of curcumin on many viruses, including SARS-CoV-2, by interacting with viral membrane proteins, disrupting the viral membrane, suppressing viral proteases, and stimulating host reactions. Moreover, by controlling numerous cellular pathways, including the nuclear factor- (NF-) κB signaling pathway, inflammasome, IL-6 trans-signaling, and HMGB1 pathways, protection from lethal pneumonia and acute respiratory distress syndrome (ARDS), ubiquitin-proteasome mechanism, and cellular post-transcriptional and post-translational alterations.[6,161,162] Curcumin is considered harmless and well tolerated in both normal and infected humans. Therefore, the fabricated curcumin transferosomes in-situ gel formulation is a promising formulation that could be used in the application against SARS-CoV-2 due to the lower cellular toxicity and enhanced antiviral efficacy. Furthermore, the developed formulation can circumvent the obstacles that restrict the use of curcumin as an efficient antiviral agent for managing COVID-19.

Pharmacokinetic Study

In humans, the peroral bioavailability of curcumin is barely 1%, primarily because it is poorly water-soluble[163] and rapidly metabolized via conjugation to generate its glucuronide or sulfate moieties. Furthermore, extensive systemic clearance may be another factor that contributes to the limited bioavailability of curcumin. Consequently, it remains virtually unnoticeable in target tissues.[164–166] In addition, curcumin was rapidly degraded into various ineffective byproducts at a physiological pH.[167] We postulated that curcumin encapsulated in transferosome vesicles laden with a thermosensitive in situ gel could augment curcumin bioavailability and delivery efficacy to the lung after intranasal treatment. The cavity of the nose is characterized by porous mucosa and many capillaries in the lamina propria, which can enhance the transmucosal uptake of therapeutics.[168,169] In addition, the long residential period attributed to the gel viscosity, small hydrodynamic diameter, and augmented penetration efficacy of Transcutol across the nasal membrane could be beneficial for enhancing curcumin absorption in the nasal cavity.[39,111]

The linear range for the suggested fluorometric technique for assaying the curcumin in spiked plasma was 20.0–350.0 ng mL^{-1} with the regression formula (y = 3.36 X - 2.14). The detection (LOD) and the quantitation (LOQ) limits were 6.53 ng mL^{-1} and 19.80 ng mL^{-1}, respectively.

The average curcumin plasma level–time profiles after intranasal administration of curcumin transferosome-incorporated in situ gel (5 mg/kg) and free curcumin-incorporated in situ gel (5 mg/kg) are shown in Figure S2. The relevant pharmacokinetic data were estimated and are presented in Table 5. Following intranasal administration, the maximum curcumin concentration in plasma was recorded in the group receiving curcumin transferosome in situ gel formulation (77.348 ± 0.577 ng/mL) as opposed to the free curcumin in situ gel group (65.521 ± 0.984 ng/mL) ($p < 0.0001$). The duration needed to attain the maximum concentration (T_{max}) was 3 h and 2 h for the group receiving curcumin transferosome in situ gel formulation and free curcumin in situ gel formulation, respectively ($p = 0.0003$). The bioavailability of the medication correlated with the area under the concentration-time curve ($AUC_{0-\infty}$). $AUC_{0-\infty}$ was determined to be substantially higher for the proposed curcumin transferosome in situ gel formulation (4857.366 ± 228.240 ng/mL*h) than for the free curcumin in situ gel formula (2145.692 ± 237.514 ng/mL*h) ($p = 0.0001$). Furthermore, the relative bioavailability was enhanced (226.45%) for curcumin transferosome in-situ gel preparation versus free curcumin in-situ gel formula after intranasal administration to rabbits. This finding supports the therapeutic impact of the developed formulation and a significant improvement in its bioavailability. In addition, longer MRT values (2.5 times) higher were estimated for the group acquiring curcumin transferosomes in situ gel preparation, in contrast to the free drug in situ gel group. This observation confirmed the prolonged effect of the developed transferosomal in situ gel preparation method. The clearance of curcumin from the formulated transferosomal in situ gel was 2.3- fold lower than that of the free curcumin gel. Higher plasma concentration, extended MRT, lower drug clearance, and higher $AUC_{0-\infty}$ estimated for transferosomal in situ gel versus free drug-in situ gel confirmed longer drug retention duration, prolonged drug release, delayed elimination, excellent bioavailability enhancement, and improved therapeutic efficacy of the developed formula.

The considerable increase in the half-life ($t_{1/2}$) of both intranasal formulations is attributed to the retardation of curcumin release due to the use of the gelling system. However, the higher retardation exhibited by the transferosome gel formulation may be due to the dual sustained actions of both the gelling and vesicular systems.[141]

The large extent of drug absorption from the optimized curcumin transferosomes in situ gel, in contrast with the free curcumin in situ gel, as shown by significant increases in C_{max} and AUC, could be elucidated based on the drug's enhanced permeability and solubility by embedding within a hydrophobic carrier. In addition, the enhanced permeation properties of transferosomes due to their deformability and flexibility can improve permeation across the mucosal barrier.[108,147] Moreover, the shielding effect of nanoscale transferosomes may protect the drug from rapid excretion and metabolism.[170] The shielding effect of transferosomes may be attributed to the efficient encapsulation of curcumin within the lipid vesicles, which offers maximized drug protection against degradation, prolonged residence time at the nasal mucosa, extended circulation of the drug in the blood, extended half-life of the drug, and suppressed rapid

Table 5 Pharmacokinetic Parameters in Plasma Following Intranasal Administration of Curcumin Transferosomes in-situ Gel and Free Curcumin in-situ Gel Formulations

Formulation	C_{max} (ng/mL)	T_{max} (h)	AUC_{0-t} (ng/mL*h)	$AUC_{0-\infty}$ (ng/mL*h)	$MRT_{0\text{-}inf\_obs}$ (h)	$Cl/F_{\_obs}$ (ng)/(ng/mL)/h	$t_{1/2}$(h)
Curcumin transferosomes in-situ gel	77.348 ± 0.577****	3 ± 0.1***	519.954 ± 4.00^{ns}	4857.366 ± 228.240***	115.914± 3.524****	2061.742± 96.218***	81.203± 2.167****
Free curcumin in-situ gel	65.521 ± 0.984	2 ± 0.1	513.978 ± 13.438	2145.692 ± 237.514	45.539± 5.203	4697.607± 503.562	31.967± 3.718

Notes: ***Extremely significant different ($p < 0.001$). **** Extremely significant different ($p < 0.0001$). ^{ns} Non-significant difference compared to free curcumin in situ gel ($p > 0.05$). Statistical significance was computed using Student's *t*-test. Results are represented as the mean ±S.D.

Abbreviations: C_{max}, peak plasma concentration; (T_{max}), time to reach maximum plasma drug concentration; AUC_{0-t}, area under the plasma concentration-time curve up to definite time; $AUC_{0-\infty}$, area under the plasma concentration-time curve up to infinity; CL, plasma clearance; MRT, mean residence time ($t_{1/2}$), half-life.

clearance from the bloodstream compared to free un-entrapped drug owing to the nano-size of transferosomes and the lipid bilayer stability.

These outcomes are consistent with the findings of Ahmed et al,[147] who compared the bioavailability following intranasal application of a flibanserin-transferosome-loaded hydrogel with the control flibanserin-loaded hydrogel. The results revealed the increased bioavailability (400.22%) of drug-loaded transferosomal gel, resulting from extended residence time and enhanced permeation.

The biodistribution of curcumin following the intranasal application of curcumin transferosomes loaded in situ gel and the control curcumin entrapped in situ gel preparations to rabbits was monitored, and fluorescence was detected in different tissues after 3 h and 12 h of administration. The results are presented in Figure 12A and B.

Following the intranasal application of in situ gels comprising either curcumin transferosomes or free curcumin to rabbits, the drug was observed to persistently accumulate in the lungs, heart, trachea, kidney, liver, and brain 3 and 12 h after administration. This observation indicates that the developed curcumin formulations are bioavailable in various organs, and their accessibility declines over time, depending on the organ.[171–173]

Both curcumin preparations enhanced overall drug accumulation in the lungs at 3 h and persisted until 12 h. Curcumin transferosome-loaded in situ gel showed significantly higher lung drug accumulation (253.329 ± 0.0 ng/mL. g) than that of the free curcumin-loaded in situ gel (211.255 ± 2.77 ng/mL. g); ($p < 0.0001$) after; 3h of intranasal

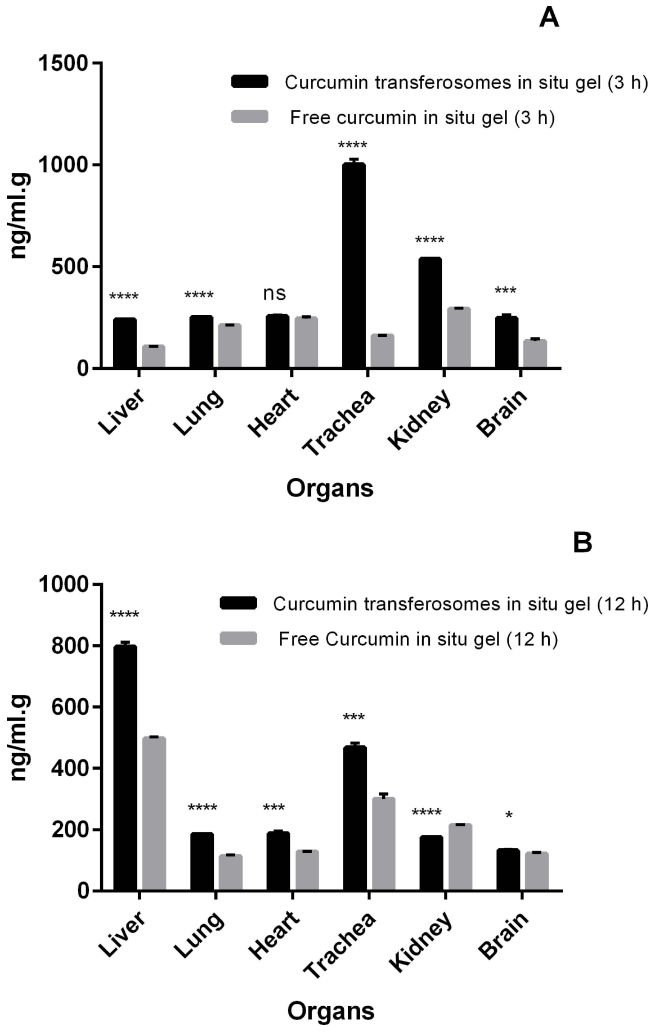

Figure 12 Biodistribution of curcumin transferosomes in-situ gel and free curcumin in-situ gel in rabbits after 3 h of administration (**A**), and after 12 h of administration (**B**). *Significantly different from free curcumin in-situ gel control ($p < 0.05$). ***Extremely significant different ($p < 0.001$). ****Extremely significant different ($p < 0.0001$). ^{ns}Non-significant difference compared to free curcumin in-situ gel ($p > 0.05$). The statistical significance was computed by Student's *t*-test.

drug administration. The results revealed that the drug was still detected in the lungs at 12 h after administration. Curcumin transferosome-loaded in situ gel showed a lung accumulation of (185.556 ± 0.000003 ng/mL. g), and the free curcumin-loaded in situ gel showed a lung accumulation of (113.652 ± 4.622 ng/mL. g) after 12 h, ($p < 0.0001$). These findings suggest that the developed curcumin transferosome gel formulation has lung deposition characteristics, indicating a therapeutic impact in lung diseases.[174]

Curcumin is considered a perfect therapeutic option for inflammation and oxidative stress disorders in the lungs owing to its multifunctional properties. The drug can avoid the free radicals of hydroxyl, nitric oxide, and superoxide radicals. It also indirectly downregulates the expression of multiple pro-inflammatory cytokines, including IFN-, IL-6, and IL-8, by deactivating Nuclear factor kappa B (NF-κB) in the lungs.[175,176] Furthermore, in many cases, secondary bacterial infections exacerbate viral respiratory infections. Curcumin protects the patients from lethal pneumonia associated with bacterial infections.[6,177] In addition, the inclusion of curcumin in transferosomes provides adequate protection and overcomes its limited water solubility, hindering the achievement of therapeutic concentrations in the lungs. In addition, as the physiological pH is between 5.5–6.5, thus curcumin can be detected in the plasma and delivered to the lung without degradation. The accumulation of curcumin into the lung epithelia while loaded within transferosomes is advantageous because of the well-established ability of phospholipids to aid the passage and penetration of therapeutics across biological barriers.[178] The in vivo biodistribution investigation demonstrated the higher efficiency of curcumin transferosome-loaded in situ gel preparation compared to the control (free drug-loaded in situ gel) as a lung delivery system.

In another study, the anti-asthmatic potential was reported after intranasal administration of curcumin at a dose of 5 mg/kg because of its suppression of inflammatory cell recruitment to the lungs and inhibition of bronchoconstriction.[64]

Maria Letizia Manca et al[175] previously examined the incorporation of curcumin into glycerosomes. Increased deposition of curcumin in the lungs of rats was demonstrated by in vivo studies, suggesting its potential utility in managing pulmonary illnesses.

Drug deposition in the trachea was significantly higher in rabbits receiving curcumin transferosome-loaded in situ gel (1002.131 ± 26.270 ng/mL. g) than that in the group that received free curcumin-loaded in situ gel (161.488 ± 1.246 ng/mL. g) after; 3 h, ($p < 0.0001$). After 12 h, curcumin transferosome-loaded in situ gel showed a maximum tracheal accumulation of (467.523± 15.443 ng/mL. g) compared with (300.457± 16.482 ng/mL. g) in the group that received control curcumin in situ gel ($p = 0.0002$).

For both tested formulations, curcumin was detected in the liver and kidney, where the liver is the main site of curcumin metabolism.[179] The amount of drug found in the liver was (240.164 ± 3.267 and 107.136 ± 1.749 ng/mL.g, respectively), ($p < 0.0001$) after; 3 h, and (796.737 ± 15.257, 497.854 ± 5.300 ng/mL.g) ($p < 0.0001$) after 12 h of administration of the curcumin transferosome gel and free curcumin gel, respectively. Drug accumulation in the kidney was determined to be (538.262 ± 3.254 and 293.061 ± 2.926 ng/mL.g, respectively), ($p < 0.0001$) after; 3 h, and (175.215 ± 2.724, 214.404 ± 3.064 ng/mL.g); ($p < 0.0001$) after 12 h of application of curcumin transferosomes and free curcumin in situ gels, respectively. There was no significant variation in the distribution of either curcumin transferosomes or free curcumin in situ gellings to the heart after 3 h of administration ($p = 0.1160$). However, the difference was significant at the end of the 12 h test ($p=0.0002$).

Curcumin brain accumulation was significantly higher in the group receiving curcumin transferosome-loaded in situ gel (247.890 ± 17.003 ng/mL. g) than in the group that received free curcumin-loaded in situ gel (134.113 ± 11.274 ng/mL. g) after; 3 h, ($p = 0.0006$). After 12 h, the curcumin transferosome-loaded in situ gel showed a brain accumulation of (132.064 ± 2.972 ng/mL. g) compared to (121.149 ± 4.194 ng/mL. g) in the group treated with the free curcumin in situ gel ($p = 0.0212$). The intranasal administration of drugs resulted in the highest level of brain permeation. This fact is ascribed to three proposed tracks: (a) the trigeminal neural pathway and (b) the olfactory pathway, by which active constituents migrate directly to the brain tissue and CSF from the nasal cavity. Moreover, the third track is the systemic path by which certain active constituents are absorbed into the bloodstream and penetrate the blood-brain barrier to target the brain.[180]

The incorporation of curcumin into nanostructured lipid carriers has been previously reported by Madane and Mahajan.[181] Upon intranasal administration, a significant improvement in the transport of curcumin to the brain from

the fabricated nanostructured lipid carriers was observed, in contrast to simple drug dispersion. This observation was due to the quick absorption and extended duration of residence of the lipid nanoparticles in the nasal cavity of the rats. Curcumin-loaded amylolipid nanoparticles were fabricated using Sintov.[182] High brain curcumin levels were recorded one hour after intranasal administration. However, no drug was detected in the brain 1 h after the intravenous delivery of a similar dose. Comparing our results with those of another study that investigated curcumin amounts in the plasma and brain following intranasal delivery of curcumin solution, curcumin-entrapped chitosan-coated poly (lactic-co-glycolic acid) nanoparticles, and curcumin/hydroxypropyl-β-cyclodextrin inclusion complexes at a dose (2 mg/kg) in mice.[165] Our results showed a much higher plasma concentration and a residence time of 24 h. These findings further proved that intranasal application of curcumin nanovesicles could enhance its bioavailability, offer a prolonged release, and facilitate drug distribution in different tissues.

Based on the aforementioned experimental results, optimum curcumin transferosome-loaded in situ gel preparation could enhance drug residence and improve its bioavailability and lung accumulation properties. These characteristics allow curcumin to directly interact with SARS-CoV-2, deliver a high concentration of curcumin to the infection site, and directly deposit into the lower airways. It is worth mentioning that, up till now, only three research investigations have examined the in vivo effectiveness of oral curcumin-encapsulated nano-based systems in COVID-19 patients.[24,127,183] Despite these encouraging outcomes, the formulations focused on mediating inflammatory responses and reducing infection symptoms. It is essential to highlight that nanodelivery systems have many characteristics that may offer additional benefits and clinical effectiveness in therapeutic management involving curcumin.

Histopathology

Histopathological examination was performed to evaluate the influence of the optimum curcumin-loaded transferosome in situ gel on rabbit nasal mucosa, in contrast with the free curcumin-entrapped in situ gel and the untreated control group. As shown in Figure S3A, the mucosa of the nose of untreated control rabbits displayed intact pseudostratified columnar epithelium with numerous goblet cells with a normal appearance. In the group treated with either free curcumin-entrapped in situ gel or the formulated curcumin transferosome in situ gel formulation (Figure S3B and C), a normal and healthy surface epithelial layer (white arrows) with fewer goblet cells (thin black arrows) was observed. Signs of necrosis or pathological abnormalities were not observed. Therefore, the curcumin transferosome in situ gel can exhibit excellent nasal tolerance and is thus considered safe for intranasal application.

Conclusion

According to an in silico docking study, curcumin could concurrently bind to the main enzymes of SARS-CoV-2. However, low bioavailability and rapid metabolism of the drug compromise its effectiveness as an antiviral compound. An optimized curcumin formulation can guarantee improved transport to the target cells and enhance cellular absorption. In this study, an intranasal thermosensitive Cur transferosomal in situ gel was formulated and evaluated. Based on the desirability approach, the transferosomes of optimum composition demonstrated a high entrapment efficiency (82.829 ± 0.023%), negative zeta potential, and nanosized vesicle size. Loading transferosomes into the in situ gel network led to enhanced and more controlled drug release, in contrast to the free curcumin incorporated into the in situ gel or transferosomes. In addition, a noticeable improvement (2.58-fold) in the amount of drug transported through the nasal mucosa of sheep was recorded for the transferosome in situ gel preparation compared with that from free curcumin gel. A curcumin transferosome-loaded in situ gel system displayed considerable anti-SARS-CoV2 potency in Vero E6 cells with minimal cellular toxicity, confirming the role of curcumin nanovesicles in inhibiting both viral entry and replication. Significant enhancements in the relative bioavailability (226.45%) and MRT (2.5 folds) of the developed formula compared to free curcumin in-situ gel have also been demonstrated after intranasal administration to rabbits. Notably, improved drug solubility and permeation properties following encapsulation within ultra-deformable vesicles enhance penetration across the mucosal barrier, thus improving drug availability. The results of the in vitro cell cytotoxicity study, in vitro antiviral efficacy test, and pharmacokinetic study highlight the potential of the combination of transferosomes as drug carriers and the in situ gel system in the improvement of antiviral treatment outcomes with curcumin. Moreover, this study clearly suggests that intranasal route provides a safe, efficient, and convenient route of pulmonary drug delivery.

Consequently, our conclusions provide an optimistic formulation that can be clinically tested as antiviral medicine for COVID-19 patients. Future perspectives will focus on examining different techniques for improvement of the stability of curcumin transferosomes vesicles to withstand variable storage conditions for a prolonged time. Besides, investigating various mechanisms involved in the cellular uptake of nanovesicles to develop safe and effective nanomedicines can be done. Moreover, evaluating the feasibility of conjugating the developed curcumin transferosomes in situ gel formulation with lung-targeting ligands, peptides, or stimuli-responsive polymer for a more enhanced lung targeting specificity can be performed. Targeted nanocarriers with surface modifications can evade immune recognition and ensure the delivery of therapeutic compounds to the target cell, hence improving cellular uptake and efficacy. Moreover, exploring the stealth functionality of polyethylene glycol (PEG) coating to prevent phagocytosis of the nanocarrier can be studied.

Acknowledgment

The authors thank Prof. Dr. Abdelaziz Abualfadl Abdelaziz Faculty of Science, Physics Department, Assiut University, Assiut, Egypt, for helping in the DSC analysis.

Author Contributions

All authors made a significant contribution to the work reported, whether that is in the conception, study design, execution, acquisition of data, analysis and interpretation, or in all these areas; took part in drafting, revising or critically reviewing the article; gave final approval of the version to be published; have agreed on the journal to which the article has been submitted; and agree to be accountable for all aspects of the work.

Funding

This research received no external funding.

Disclosure

The authors declare that they have no known competing financial interests or personal relationships that could influence the work reported in this study.

References

1. Varahachalam SP, Lahooti B, Chamaneh M, et al. Nanomedicine for the SARS-CoV-2: state-of-The-art and future prospects. *Int J Nanomedicine*. 2021;16:539. doi:10.2147/IJN.S283686
2. Ochani RK, Yasmin F, Jatoi NN. Epidemic amidst the coronavirus disease-19 pandemic. *J Glob Health*. 2021;11. doi:10.7189/jogh.11.03056
3. World Health Organization. Coronavirus disease (COVID-19); 2021; 2021.
4. Zheng C, Shao W, Chen X, Zhang B, Wang G, Zhang W. Real-world effectiveness of COVID-19 vaccines: a literature review and meta-analysis. *Int J Infectious Dis*. 2022;114:252–260. doi:10.1016/j.ijid.2021.11.009
5. Paliwal P, Sargolzaei S, Bhardwaj SK, Bhardwaj V, Dixit C, Kaushik A. Grand challenges in bio-nanotechnology to manage the COVID-19 pandemic. *Front Nanotechnol*. 2020;2:571284. doi:10.3389/fnano.2020.571284
6. Thimmulappa RK, Mudnakudu-Nagaraju KK, Shivamallu C, et al. Antiviral and immunomodulatory activity of curcumin: a case for prophylactic therapy for COVID-19. *Heliyon*. 2021;7(2):e06350. doi:10.1016/j.heliyon.2021.e06350
7. Yuki K, Fujiogi M, Koutsogiannaki S. COVID-19 pathophysiology: a review. *Clin immunol*. 2020;215:108427. doi:10.1016/j.clim.2020.108427
8. Kaushik A. Manipulative magnetic nanomedicine: the future of COVID-19 pandemic/endemic therapy. *Expert Opin Drug Deliv*. 2021;18 (5):531–534. doi:10.1080/17425247.2021.1860938
9. Fu L, Wang B, Yuan T, et al. Clinical characteristics of coronavirus disease 2019 (COVID-19) in China: a systematic review and meta-analysis. *J Infection*. 2020;80(6):656–665. doi:10.1016/j.jinf.2020.03.041
10. Chan JF-W, Yuan S, Kok K-H, et al. A familial cluster of pneumonia associated with the 2019 novel coronavirus indicating person-to-person transmission: a study of a family cluster. *Lancet*. 2020;395(10223):514–523. doi:10.1016/S0140-6736(20)30154-9
11. Guo T, Fan Y, Chen M, et al. Cardiovascular implications of fatal outcomes of patients with coronavirus disease 2019 (COVID-19). *JAMA cardiol*. 2020;5(7):811–818. doi:10.1001/jamacardio.2020.1017
12. Wang M, Cao R, Zhang L, et al. Remdesivir and chloroquine effectively inhibit the recently emerged novel coronavirus (2019-nCoV) in vitro. *Cell Res*. 2020;30(3):269–271. doi:10.1038/s41422-020-0282-0
13. Chen J, Liu D, Liu L, et al. A pilot study of hydroxychloroquine in treatment of patients with moderate COVID-19. *J Zhejiang Univ*. 2020;49 (2):215–219.
14. Chu C, Cheng V, Hung I, et al. Role of lopinavir/ritonavir in the treatment of SARS: initial virological and clinical findings. *Thorax*. 2004;59 (3):252–256. doi:10.1136/thorax.2003.012658
15. Tanaka T, Narazaki M, Kishimoto T. Immunotherapeutic implications of IL-6 blockade for cytokine storm. *Immunotherapy*. 2016;8(8):959–970. doi:10.2217/imt-2016-0020

16. Zhai P, Ding Y, Wu X, Long J, Zhong Y, Li Y. The epidemiology, diagnosis and treatment of COVID-19. *Int J Antimicrob Agents*. 2020;55(5):105955. doi:10.1016/j.ijantimicag.2020.105955
17. Benvenuto D, Giovanetti M, Ciccozzi A, Spoto S, Angeletti S, Ciccozzi M. The 2019-new coronavirus epidemic: evidence for virus evolution. *J Med Virol*. 2020;92(4):455–459. doi:10.1002/jmv.25688
18. Moore JB, June CH. Cytokine release syndrome in severe COVID-19. *Science*. 2020;368(6490):473–474. doi:10.1126/science.abb8925
19. Di Stadio A, Ishai R, Gambacorta V, et al. Nutraceuticals as immune-stimulating therapy to fight COVID-19. Combination of elements to improve the efficacy. *Eur Rev Med Pharmacol Sci*. 2020;24(17):56.
20. Dubey AK, Chaudhry SK, Singh HB, Gupta VK, Kaushik A. Perspectives on nano-nutraceuticals to manage pre and post COVID-19 infections. *Biotechnol Rep*. 2022;33:e00712. doi:10.1016/j.btre.2022.e00712
21. Lelli D, Sahebkar A, Johnston TP, Pedone C. Curcumin use in pulmonary diseases: state of the art and future perspectives. *Pharmacol Res*. 2017;115:133–148. doi:10.1016/j.phrs.2016.11.017
22. Varthya SB, Thangaraju P, Venkatesan S. Curcumin and fungal infection–commonly available herbs for common female infection. *J Family Med Primary Care*. 2020;9(2):1272. doi:10.4103/jfmpc.jfmpc_1218_19
23. Wen -C-C, Kuo Y-H, Jan J-T, et al. Specific plant terpenoids and lignoids possess potent antiviral activities against severe acute respiratory syndrome coronavirus. *J Med Chem*. 2007;50(17):4087–4095. doi:10.1021/jm070295s
24. Valizadeh H, Abdolmohammadi-Vahid S, Danshina S, et al. Nano-curcumin therapy, a promising method in modulating inflammatory cytokines in COVID-19 patients. *Int Immunopharmacol*. 2020;89:107088. doi:10.1016/j.intimp.2020.107088
25. Nemmar A, Subramaniyan D, Ali BH. Protective effect of curcumin on pulmonary and cardiovascular effects induced by repeated exposure to diesel exhaust particles in mice. *PLoS One*. 2012;7(6):e39554. doi:10.1371/journal.pone.0039554
26. Y-s C, Y-q C, S-h L, et al. Curcumin regulates the differentiation of naïve CD4+ T cells and activates IL-10 immune modulation against acute lung injury in mice. *Biomed Pharmacother*. 2020;125:109946. doi:10.1016/j.biopha.2020.109946
27. Zahedipour F, Hosseini SA, Sathyapalan T, et al. Potential effects of curcumin in the treatment of COVID-19 infection. *Phytother Res*. 2020;34(11):2911–2920. doi:10.1002/ptr.6738
28. Dourado D, Freire DT, Pereira DT, et al. Will curcumin nanosystems be the next promising antiviral alternatives in COVID-19 treatment trials? *Biomed Pharmacother*. 2021;139:111578. doi:10.1016/j.biopha.2021.111578
29. Liu W, Zhai Y, Heng X, et al. Oral bioavailability of curcumin: problems and advancements. *J Drug Target*. 2016;24(8):694–702. doi:10.3109/1061186X.2016.1157883
30. Jyoti J, Anandhakrishnan NK, Singh SK, et al. A three-pronged formulation approach to improve oral bioavailability and therapeutic efficacy of two lipophilic drugs with gastric lability. *Drug Deliv Transl Res*. 2019;9(4):848–865. doi:10.1007/s13346-019-00635-0
31. Chauhan G, Madou MJ, Kalra S, Chopra V, Ghosh D, Martinez-Chapa SO. Nanotechnology for COVID-19: therapeutics and vaccine research. *ACS nano*. 2020;14(7):7760–7782. doi:10.1021/acsnano.0c04006
32. Sood S, Jain K, Gowthamarajan K. Optimization of curcumin nanoemulsion for intranasal delivery using design of experiment and its toxicity assessment. *Colloids Surf B Biointerfaces*. 2014;113:330–337. doi:10.1016/j.colsurfb.2013.09.030
33. de Barros C, Portugal I, Batain F, et al. Formulation, design and strategies for efficient nanotechnology-based nasal delivery systems. *RPS Pharm Pharmacol Rep*. 2022;1(1):rqac003. doi:10.1093/rpsppr/rqac003
34. Khan K, Aqil M, Imam SS, et al. Ursolic acid loaded intra nasal nano lipid vesicles for brain tumour: formulation, optimization, in-vivo brain/plasma distribution study and histopathological assessment. *Biomed Pharmacother*. 2018;106:1578–1585. doi:10.1016/j.biopha.2018.07.127
35. Marasini N, Kaminskas LM. Subunit-based mucosal vaccine delivery systems for pulmonary delivery-Are they feasible? *Drug Dev Ind Pharm*. 2019;45(6):882–894. doi:10.1080/03639045.2019.1583758
36. Sung JC, Pulliam BL, Edwards DA. Nanoparticles for drug delivery to the lungs. *Trends Biotechnol*. 2007;25(12):563–570. doi:10.1016/j.tibtech.2007.09.005
37. Hosny KM, Rizg WY, Khallaf RA. Preparation and optimization of in situ gel loaded with rosuvastatin-ellagic acid nanotransfersomes to enhance the anti-proliferative activity. *Pharmaceutics*. 2020;12(3):263. doi:10.3390/pharmaceutics12030263
38. Opatha SAT, Titapiwatanakun V, Chutoprapat R. Transfersomes: a promising nanoencapsulation technique for transdermal drug delivery. *Pharmaceutics*. 2020;12(9):855. doi:10.3390/pharmaceutics12090855
39. Pitta SK, Dudhipala N, Narala A, Veerabrahma K. Development of zolmitriptan transfersomes by Box–Behnken design for nasal delivery: in vitro and in vivo evaluation. *Drug Dev Ind Pharm*. 2018;44(3):484–492. doi:10.1080/03639045.2017.1402918
40. ElShagea HN, Makar RR, Salama AH, Elkasabgy NA, Basalious EB. Investigating the Targeting Power to Brain Tissues of Intranasal Rasagiline Mesylate-Loaded Transferosomal In Situ Gel for Efficient Treatment of Parkinson's Disease. *Pharmaceutics*. 2023;15(2):533. doi:10.3390/pharmaceutics15020533
41. Allam A, Elsabahy M, El Badry M, Eleraky NE. Betaxolol-loaded niosomes integrated within pH-sensitive in situ forming gel for management of glaucoma. *Int J Pharm*. 2021;598:120380. doi:10.1016/j.ijpharm.2021.120380
42. Chen Y, Lee J-H, Meng M, et al. An overview on thermosensitive oral gel based on poloxamer 407. *Materials*. 2021;14(16):4522. doi:10.3390/ma14164522
43. Joshi A, Kaur J, Kulkarni R, Chaudhari R. In-vitro and ex-vivo evaluation of raloxifene hydrochloride delivery using nano-transfersome based formulations. *J Drug Deliv Sci Technol*. 2018;45:151–158. doi:10.1016/j.jddst.2018.02.006
44. Clogston JD, Patri AK. Zeta potential measurement. *Characterization Nanoparticles Intended Drug Delivery*. 2011;63–70.
45. Badr-Eldin SM, Ahmed OA. Optimized nano-transfersomal films for enhanced sildenafil citrate transdermal delivery: ex vivo and in vivo evaluation. *Drug Des Devel Ther*. 2016;10:1323. doi:10.2147/DDDT.S103122
46. Wei G, Xu H, Ding PT, Zheng JM, Zheng JM. Thermosetting gels with modulated gelation temperature for ophthalmic use: the rheological and gamma scintigraphic studies. *J Controlled Release*. 2002;83(1):65–74. doi:10.1016/S0168-3659(02)00175-X
47. Qi H, Chen W, Huang C, et al. Development of a poloxamer analogs/carbopol-based in situ gelling and mucoadhesive ophthalmic delivery system for puerarin. *Int J Pharm*. 2007;337(1–2):178–187. doi:10.1016/j.ijpharm.2006.12.038
48. Abdel Bary G. Preparation and Characterization of Thermosensitive Mucoadhesive In_Situ Gels for Nasal Delivery of Ondansetron Hydrochloride. *Al-Azhar J Pharm Sci*. 2014;50(2):191–207. doi:10.21608/ajps.2014.6953

49. Brambilla E, Locarno S, Gallo S, et al. Poloxamer-based hydrogel as drug delivery system: how polymeric excipients influence the chemical-physical properties. *Polymers*. 2022;14(17):3624. doi:10.3390/polym14173624
50. Choi H-G, Jung J-H, Ryu J-M, Yoon S-J, Y-K O, Kim C-K. Development of in situ-gelling and mucoadhesive Acetaminophen liquid suppository. *Int J Pharm*. 1998;165(1):33–44. doi:10.1016/S0378-5173(97)00386-4
51. Hirun N, Kraisit P, Tantishaiyakul V. Thermosensitive Polymer Blend Composed of Poloxamer 407, Poloxamer 188 and Polycarbophil for the Use as Mucoadhesive In Situ Gel. *Polymers*. 2022;14(9):1836. doi:10.3390/polym14091836
52. Soliman GM, Fetih G, Abbas AM. Thermosensitive bioadhesive gels for the vaginal delivery of sildenafil citrate: in vitro characterization and clinical evaluation in women using clomiphene citrate for induction of ovulation. *Drug Dev Ind Pharm*. 2017;43(3):399–408. doi:10.1080/03639045.2016.1254239
53. Mekkawy AI, Eleraky NE, Soliman GM, Elnaggar MG, Elnaggar MG. Combinatorial Therapy of Letrozole-and Quercetin-Loaded Spanlastics for Enhanced Cytotoxicity against MCF-7 Breast Cancer Cells. *Pharmaceutics*. 2022;14(8):1727. doi:10.3390/pharmaceutics14081727
54. Fathalla Z, Mustafa WW, Abdelkader H, Moharram H, Sabry AM, Alany RG. Hybrid thermosensitive-mucoadhesive in situ forming gels for enhanced corneal wound healing effect of L-carnosine. *Drug Deliv*. 2022;29(1):374–385. doi:10.1080/10717544.2021.2023236
55. Allam AA, Eleraky NE, Diab NH, et al. Development of Sedative Dexmedetomidine Sublingual In Situ Gels: In vitro and In Vivo Evaluations. *Pharmaceutics*. 2022;14(2):220. doi:10.3390/pharmaceutics14020220
56. Mircioiu C, Voicu V, Anuta V, et al. Mathematical modeling of release kinetics from supramolecular drug delivery systems. *Pharmaceutics*. 2019;11(3):140. doi:10.3390/pharmaceutics11030140
57. Verekar RR, Gurav SS, Bolmal U. Thermosensitive mucoadhesive in situ gel for intranasal delivery of Almotriptan malate: formulation, characterization, and evaluation. *J Drug Deliv Sci Technol*. 2020;58:101778. doi:10.1016/j.jddst.2020.101778
58. Patel S, Koradia H, Parikh R. Design and development of intranasal in situ gelling system of Midazolam hydrochloride using 32 full factorial design. *J Drug Deliv Sci Technol*. 2015;30:154–162. doi:10.1016/j.jddst.2015.10.010
59. Galgatte UC, Kumbhar AB, Chaudhari PD. Development of in situ gel for nasal delivery: design, optimization, in vitro and in vivo evaluation. *Drug Deliv*. 2014;21(1):62–73. doi:10.3109/10717544.2013.849778
60. Sylvester PW. Optimization of the tetrazolium dye (MTT) colorimetric assay for cellular growth and viability. *Drug Des Discov*. 2011;2011:157–168.
61. Mostafa A, Kandeil A, Elshaier Y, et al. FDA-approved drugs with potent in vitro antiviral activity against severe acute respiratory syndrome coronavirus 2. *Pharmaceuticals*. 2020;13(12):443. doi:10.3390/ph13120443
62. Karimi M, Mashreghi M, Shokooh Saremi S, Jaafari MR. Spectrofluorometric method development and validation for the determination of curcumin in nanoliposomes and plasma. *J Fluoresc*. 2020;30(5):1113–1119. doi:10.1007/s10895-020-02574-3
63. Abdel-Lateef MA, Almahri A. Micellar sensitized Resonance Rayleigh Scattering and spectrofluorometric methods based on isoindole formation for determination of Eflornithine in cream and biological samples. *Spectrochim Acta A Mol Biomol Spectrosc*. 2021;258:119806. doi:10.1016/j.saa.2021.119806
64. Chauhan PS, Kumari S, Kumar JP, et al. Intranasal curcumin and its evaluation in murine model of asthma. *Int Immunopharmacol*. 2013;17(3):733–743. doi:10.1016/j.intimp.2013.08.008
65. E. Eleraky NM, Omar MA, Mahmoud HA, Abou-Taleb H. Nanostructured lipid carriers to mediate brain delivery of temazepam: design and in vivo study. *Pharmaceutics*. 2020;12(5):451. doi:10.3390/pharmaceutics12050451
66. Omar MM, Hasan OA, Zaki RM, Eleraky NE. Externally triggered novel rapid-release sonosensitive folate-modified liposomes for gemcitabine: development and characteristics. *Int J Nanomedicine*. 2021;16:683. doi:10.2147/IJN.S266676
67. Ahmed TA, Badr-Eldin SM, Ahmed OA, Aldawsari H. Intranasal optimized solid lipid nanoparticles loaded in situ gel for enhancing trans-mucosal delivery of simvastatin. *J Drug Deliv Sci Technol*. 2018;48:499–508. doi:10.1016/j.jddst.2018.10.027
68. Fu L, Ye F, Feng Y, et al. Both Boceprevir and GC376 efficaciously inhibit SARS-CoV-2 by targeting its main protease. *Nat Commun*. 2020;11(1):4417. doi:10.1038/s41467-020-18233-x
69. Rubin D, Chan-Tack K, Farley J, Sherwat A. FDA Approval of Remdesivir — a Step in the Right Direction. *N Eng J Med*. 2020;383(27):2598–2600. doi:10.1056/NEJMp2032369
70. Yin W, Mao C, Luan X, et al. Structural basis for inhibition of the RNA-dependent RNA polymerase from SARS-CoV-2 by remdesivir. *Science*. 2020;368(6498):1499–1504. doi:10.1126/science.abc1560
71. Li W, Moore MJ, Vasilieva N, et al. Angiotensin-converting enzyme 2 is a functional receptor for the SARS coronavirus. *Nature*. 2003;426(6965):450–454. doi:10.1038/nature02145
72. Li F. Structural analysis of major species barriers between humans and palm civets for severe acute respiratory syndrome coronavirus infections. *J Virol*. 2008;82(14):6984–6991. doi:10.1128/jvi.00442-08
73. Wu K, Peng G, Wilken M, Geraghty RJ, Li F. Mechanisms of host receptor adaptation by severe acute respiratory syndrome coronavirus. *J Biol Chem*. 2012;287(12):8904–8911. doi:10.1074/jbc.M111.325803
74. Shang J, Ye G, Shi K, et al. Structural basis of receptor recognition by SARS-CoV-2. *Nature*. 2020;581(7807):221–224. doi:10.1038/s41586-020-2179-y
75. Tamilarasan N, Yasmin BM, Anitha P, et al. Box–Behnken Design: optimization of Proanthocyanidin-Loaded Transferosomes as an Effective Therapeutic Approach for Osteoarthritis. *Nanomaterials*. 2022;12(17):2954. doi:10.3390/nano12172954
76. Uwaezuoke O, Du Toit LC, Kumar P, Ally N, Choonara YE. Linoleic Acid-Based Transferosomes for Topical Ocular Delivery of Cyclosporine A. *Pharmaceutics*. 2022;14(8):1695. doi:10.3390/pharmaceutics14081695
77. Mazyed EA, Abdelaziz AE. Fabrication of transgelosomes for enhancing the ocular delivery of Acetazolamide: statistical optimization, in vitro characterization, and in vivo study. *Pharmaceutics*. 2020;12(5):465. doi:10.3390/pharmaceutics12050465
78. Varia U, Joshi D, Jadeja M, Katariya H, Detholia K, Soni V. Development and evaluation of ultradeformable vesicles loaded transdermal film of boswellic acid. *Future J Pharm Sci*. 2022;8(1):39. doi:10.1186/s43094-022-00428-2
79. Bnyan R, Khan I, Ehtezazi T, et al. Surfactant effects on lipid-based vesicles properties. *J Pharm Sci*. 2018;107(5):1237–1246. doi:10.1016/j.xphs.2018.01.005
80. Varia U, Joshi D, Jadeja M, Katariya H, Detholia K, Soni V. Development and evaluation of ultradeformable vesicles loaded transdermal film of boswellic acid. *Future J Pharm Sci*. 2022;8(1):1–16. doi:10.1186/s43094-022-00428-2

81. Petchsomrit A, Sermkaew N, Wiwattanapatapee R. Effect of alginate and surfactant on physical properties of oil entrapped alginate bead formulation of curcumin. *Int J Pharmacol Pharmaceutical Sci*. 2013;7(12):864–868.
82. Elsheikh MA, Elnaggar YS, Hamdy DA, Abdallah OY. Novel cremochylomicrons for improved oral bioavailability of the antineoplastic phytomedicine berberine chloride: optimization and pharmacokinetics. *Int J Pharm*. 2018;535(1–2):316–324. doi:10.1016/j.ijpharm.2017.11.023
83. Ahmed TA. Preparation of transfersomes encapsulating sildenafil aimed for transdermal drug delivery: plackett–Burman design and characterization. *J Liposome Res*. 2015;25(1):1–10. doi:10.3109/08982104.2014.950276
84. El Zaafarany GM, Awad GA, Holayel SM, Mortada ND. Role of edge activators and surface charge in developing ultradeformable vesicles with enhanced skin delivery. *Int J Pharm*. 2010;397(1–2):164–172. doi:10.1016/j.ijpharm.2010.06.034
85. El-Gizawy SA, Nouh A, Saber S, Kira AY. Deferoxamine-loaded transfersomes accelerates healing of pressure ulcers in streptozotocin-induced diabetic rats. *J Drug Deliv Sci Technol*. 2020;58:101732. doi:10.1016/j.jddst.2020.101732
86. Chaudhary H, Kohli K, Kumar V. Nano-transfersomes as a novel carrier for transdermal delivery. *Int J Pharm*. 2013;454(1):367–380. doi:10.1016/j.ijpharm.2013.07.031
87. Manconi M, Sinico C, Valenti D, Loy G, Fadda AM. Niosomes as carriers for tretinoin. I. Preparation and properties. *Int J Pharm*. 2002;234(1–2):237–248. doi:10.1016/S0378-5173(01)00971-1
88. Wang Z, He X. Dynamics of vesicle formation from lipid droplets: mechanism and controllability. *J Chem Phys*. 2009;130(9):094905. doi:10.1063/1.3079097
89. Jain S, Jain P, Umamaheshwari R, Jain N. Transfersomes—a novel vesicular carrier for enhanced transdermal delivery: development, characterization, and performance evaluation. *Drug Dev Ind Pharm*. 2003;29(9):1013–1026. doi:10.1081/DDC-120025458
90. Aboud HM, Ali AA, El-Menshawe SF, Elbary AA. Nanotransfersomes of carvedilol for intranasal delivery: formulation, characterization and in vivo evaluation. *Drug Deliv*. 2016;23(7):2471–2481. doi:10.3109/10717544.2015.1013587
91. Abdelbary GA, Aburahma MH. Oro-dental mucoadhesive proniosomal gel formulation loaded with lornoxicam for management of dental pain. *J Liposome Res*. 2015;25(2):107–121. doi:10.3109/08982104.2014.941861
92. Bnyan R, Khan I, Ehtezazi T, et al. Formulation and optimisation of novel transfersomes for sustained release of local anaesthetic. *J Pharm Pharmacol*. 2019;71(10):1508–1519. doi:10.1111/jphp.13149
93. Young TJ, Johnston KP, Pace GW, Mishra AK. Phospholipid-stabilized nanoparticles of cyclosporine A by rapid expansion from supercritical to aqueous solution. *Aaps Pharmscitech*. 2004;5(1):70–85. doi:10.1208/pt050111
94. Qushawy M, Nasr A, Abd-Alhaseeb M, Swidan S. Design, optimization and characterization of a transfersomal gel using miconazole nitrate for the treatment of candida skin infections. *Pharmaceutics*. 2018;10(1):26. doi:10.3390/pharmaceutics10010026
95. Yeo LK, Olusanya TO, Chaw CS, Elkordy AA. Brief effect of a small hydrophobic drug (cinnarizine) on the physicochemical characterisation of niosomes produced by thin-film hydration and microfluidic methods. *Pharmaceutics*. 2018;10(4):185. doi:10.3390/pharmaceutics10040185
96. Rabia S, Khaleeq N, Batool S, et al. Rifampicin-loaded nanotransferosomal gel for treatment of cutaneous leishmaniasis: passive targeting via topical route. *Nanomedicine*. 2020;15(2):183–203. doi:10.2217/nnm-2019-0320
97. Studart AR, Amstad E, Gauckler LJ. Colloidal stabilization of nanoparticles in concentrated suspensions. *Langmuir*. 2007;23(3):1081–1090. doi:10.1021/la062042s
98. Ahad A, Al-Saleh AA, Al-Mohizea AM, et al. Formulation and characterization of novel soft nanovesicles for enhanced transdermal delivery of eprosartan mesylate. *Saudi Pharmaceutical j*. 2017;25(7):1040–1046. doi:10.1016/j.jsps.2017.01.006
99. Kolbina M. *Phospholipids as Functional Excipients in Solid Oral Dosage Forms*. Germany: Freie Universitaet Berlin; 2018.
100. Rachmawati H, Budiputra DK, Mauludin R. Curcumin nanoemulsion for transdermal application: formulation and evaluation. *Drug Dev Ind Pharm*. 2015;41(4):560–566. doi:10.3109/03639045.2014.884127
101. Ahad A, Al-Saleh AA, Al-Mohizea AM, et al. Formulation and characterization of Phospholipon 90 G and tween 80 based transfersomes for transdermal delivery of eprosartan mesylate. *Pharm Dev Technol*. 2018;23(8):787–793. doi:10.1080/10837450.2017.1330345
102. Sinico C, Manconi M, Peppi M, Lai F, Valenti D, Fadda AM. Liposomes as carriers for dermal delivery of tretinoin: in vitro evaluation of drug permeation and vesicle–skin interaction. *J Controlled Release*. 2005;103(1):123–136. doi:10.1016/j.jconrel.2004.11.020
103. Basha M, El-Alim SH A, Shamma RN, Awad GE. Design and optimization of surfactant-based nanovesicles for ocular delivery of Clotrimazole. *J Liposome Res*. 2013;23(3):203–210. doi:10.3109/08982104.2013.788025
104. Aziz DE, Abdelbary AA, Elassasy AI. Fabrication of novel elastosomes for boosting the transdermal delivery of diacerein: statistical optimization, ex-vivo permeation, in-vivo skin deposition and pharmacokinetic assessment compared to oral formulation. *Drug Deliv*. 2018;25(1):815–826. doi:10.1080/10717544.2018.1451572
105. Arunothayanun P, Bernard M-S, Craig D, Uchegbu I, Florence A. The effect of processing variables on the physical characteristics of non-ionic surfactant vesicles (niosomes) formed from a hexadecyl diglycerol ether. *Int J Pharm*. 2000;201(1):7–14. doi:10.1016/S0378-5173(00)00362-8
106. Malakar J, Sen SO, Nayak AK, Sen KK. Formulation, optimization and evaluation of transferosomal gel for transdermal insulin delivery. *Saudi Pharmaceutical j*. 2012;20(4):355–363. doi:10.1016/j.jsps.2012.02.001
107. Kazmi I, Al-Abbasi FA, Nadeem MS, Altayb HN, Alshehri S, Imam SS. Formulation, Optimization and Evaluation of Luteolin-Loaded Topical Nanoparticulate Delivery System for the Skin Cancer. *Pharmaceutics*. 2021;13(11):1749. doi:10.3390/pharmaceutics13111749
108. Salem HF, Kharshoum RM, Abou-Taleb HA, Naguib DM. Nanosized transferosome-based intranasal in situ gel for brain targeting of resveratrol: formulation, optimization, in vitro evaluation, and in vivo pharmacokinetic study. *Aaps pharmscitech*. 2019;20(5):1–14. doi:10.1208/s12249-019-1353-8
109. Mura P, Mennini N, Nativi C, Richichi B. In situ mucoadhesive-thermosensitive liposomal gel as a novel vehicle for nasal extended delivery of opiorphin. *Eur J Pharmaceutics Biopharmaceutics*. 2018;122:54–61. doi:10.1016/j.ejpb.2017.10.008
110. Altuntaş E, Yener G. Formulation and evaluation of thermoreversible in situ nasal gels containing mometasone furoate for allergic rhinitis. *AAPS PharmSciTech*. 2017;18(7):2673–2682. doi:10.1208/s12249-017-0747-8
111. Nair AB, Chaudhary S, Shah H, et al. Intranasal Delivery of Darunavir-Loaded Mucoadhesive In Situ Gel: experimental Design, In Vitro Evaluation, and Pharmacokinetic Studies. *Gels*. 2022;8(6):342. doi:10.3390/gels8060342
112. Durgun ME, Mesut B, Hacıoğlu M, Güngör S, Özsoy Y. Optimization of the Micellar-Based In Situ Gelling Systems Posaconazole with Quality by Design (QbD) Approach and Characterization by In Vitro Studies. *Pharmaceutics*. 2022;14(3):526. doi:10.3390/pharmaceutics14030526

113. Fathalla ZM, Vangala A, Longman M, et al. Poloxamer-based thermoresponsive ketorolac tromethamine in situ gel preparations: design, characterisation, toxicity and transcorneal permeation studies. *Eur J Pharmaceutics Biopharmaceutics*. 2017;114:119–134. doi:10.1016/j.ejpb.2017.01.008
114. Boonlai W, Tantishaiyakul V, Hirun N, Sangfai T, Suknuntha K. Thermosensitive poloxamer 407/poly (acrylic acid) hydrogels with potential application as injectable drug delivery system. *AAPS PharmSciTech*. 2018;19(5):2103–2117. doi:10.1208/s12249-018-1010-7
115. Wang Q, Wong C-H, Chan HE, Lee W-Y, Zuo Z. Statistical Design of Experiment (DoE) based development and optimization of DB213 in situ thermosensitive gel for intranasal delivery. *Int J Pharm*. 2018;539(1–2):50–57. doi:10.1016/j.ijpharm.2018.01.032
116. Zueva OS, Makarova AO, Zvereva ER, et al. Industrial block copolymer surfactants: diversity of associative forms and interaction with carbon nanomaterial. *J Mol Liq*. 2022;359:119267. doi:10.1016/j.molliq.2022.119267
117. Arkin A, Elham A, Anwar A, Kalimanjiang G, Iminjan M. Optimization and Evaluation of the Quercus infectoria Galls Thermosensitive In Situ Gel for Rectal Delivery. *Evidence Based Complementary Alternative Med*. 2022;2022. doi:10.1155/2022/8451055
118. Zhou Q, Zhong L, Wei X, Dou W, Chou G, Wang Z. Baicalein and hydroxypropyl-γ-cyclodextrin complex in poloxamer thermal sensitive hydrogel for vaginal administration. *Int J Pharm*. 2013;454(1):125–134. doi:10.1016/j.ijpharm.2013.07.006
119. Teaima MH, El Mohamady AM, El-Nabarawi MA, Mohamed AI. Formulation and evaluation of niosomal vesicles containing ondansetron HCL for trans-mucosal nasal drug delivery. *Drug Dev Ind Pharm*. 2020;46(5):751–761. doi:10.1080/03639045.2020.1753061
120. Chang JY, Oh Y-K, H-g C, Kim YB, Kim C-K. Rheological evaluation of thermosensitive and mucoadhesive vaginal gels in physiological conditions. *Int J Pharm*. 2002;241(1):155–163. doi:10.1016/S0378-5173(02)00232-6
121. El-Feky YA, Fares AR, Zayed G, El-Telbany RFA, Ahmed KA, El-Telbany DFA. Repurposing of nifedipine loaded in situ ophthalmic gel as a novel approach for glaucoma treatment. *Biomed Pharmacother*. 2021;142:112008. doi:10.1016/j.biopha.2021.112008
122. Teaima MH, Helal DA, Alsofany JM, El-Nabarawi MA, Yasser M. Ion-Triggered In Situ Gelling Intranasal Spray of Dronedarone Hydrochloride Nanocarriers: In vitro Optimization and In Vivo Pharmacokinetic Appraisal. *Pharmaceutics*. 2022;14(11):2405. doi:10.3390/pharmaceutics14112405
123. Chen X, Zou L-Q, Niu J, Liu W, Peng S-F, Liu C-M. The stability, sustained release and cellular antioxidant activity of curcumin nanoliposomes. *Molecules*. 2015;20(8):14293–14311. doi:10.3390/molecules200814293
124. Singh PK, Wani K, Kaul-Ghanekar R, Prabhune A, Ogale S. From micron to nano-curcumin by sophorolipid co-processing: highly enhanced bioavailability, fluorescence, and anti-cancer efficacy. *RSC Adv*. 2014;4(104):60334–60341. doi:10.1039/C4RA07300B
125. Salama A, Badran M, Elmowafy M, Soliman GM. Spironolactone-loaded leciplexes as potential topical delivery systems for female acne: in vitro appraisal and ex vivo skin permeability studies. *Pharmaceutics*. 2019;12(1):25. doi:10.3390/pharmaceutics12010025
126. Sahoo S, Chakraborti CK, Mishra SC. Qualitative analysis of controlled release ciprofloxacin/carbopol 934 mucoadhesive suspension. *J Adv Pharm Technol Res*. 2011;2(3):195. doi:10.4103/2231-4040.85541
127. Tahmasebi S, El-Esawi MA, Mahmoud ZH, et al. Immunomodulatory effects of Nanocurcumin on Th17 cell responses in mild and severe COVID-19 patients. *J Cell Physiol*. 2021;236(7):5325–5338. doi:10.1002/jcp.30233
128. Arun Raj R, Murali A. Formulation and Evaluation of Curcumin Loaded Transferosomal Nasal In-Situ Gel for Alzheimer's Disease. *Res Rev AJ Drug Formul Dev Prod*. 2019;6(2):19–31.
129. Bonaccorso A, Gigliobianco MR, Pellitteri R, et al. Optimization of curcumin nanocrystals as promising strategy for nose-to-brain delivery application. *Pharmaceutics*. 2020;12(5):476. doi:10.3390/pharmaceutics12050476
130. El-Sayed MM, Hussein AK, Sarhan HA, Mansour HF. Flurbiprofen-loaded niosomes-in-gel system improves the ocular bioavailability of flurbiprofen in the aqueous humor. *Drug Dev Ind Pharm*. 2017;43(6):902–910. doi:10.1080/03639045.2016.1272120
131. Sanidad KZ, Sukamtoh E, Xiao H, McClements DJ, Zhang G. Curcumin: recent advances in the development of strategies to improve oral bioavailability. *Annu Rev Food Sci Technol*. 2019;10:597–617. doi:10.1146/annurev-food-032818-121738
132. Manconi M, Caddeo C, Sinico C, et al. Ex vivo skin delivery of diclofenac by transcutol containing liposomes and suggested mechanism of vesicle–skin interaction. *Eur J Pharmaceutics Biopharmaceutics*. 2011;78(1):27–35. doi:10.1016/j.ejpb.2010.12.010
133. Mahajan HS, Gattani S. In situ gels of metoclopramide hydrochloride for intranasal delivery: in vitro evaluation and in vivo pharmacokinetic study in rabbits. *Drug Deliv*. 2010;17(1):19–27. doi:10.3109/10717540903447194
134. Abdellatif AA, Tawfeek HM. Transfersomal nanoparticles for enhanced transdermal delivery of clindamycin. *Aaps Pharmscitech*. 2016;17(5):1067–1074. doi:10.1208/s12249-015-0441-7
135. Al-Mahallawi AM, Khowessah OM, Shoukri RA. Nano-transfersomal ciprofloxacin loaded vesicles for non-invasive trans-tympanic ototopical delivery: in-vitro optimization, ex-vivo permeation studies, and in-vivo assessment. *Int J Pharm*. 2014;472(1–2):304–314. doi:10.1016/j.ijpharm.2014.06.041
136. Elkomy MH, El Menshawe SF, Abou-Taleb HA, Elkarmalawy MH. Loratadine bioavailability via buccal transferosomal gel: formulation, statistical optimization, in vitro/in vivo characterization, and pharmacokinetics in human volunteers. *Drug Deliv*. 2017;24(1):781–791. doi:10.1080/10717544.2017.1321061
137. Elsenosy FM, Abdelbary GA, Elshafeey AH, Elsayed I, Fares AR. Brain targeting of duloxetine HCL via intranasal delivery of loaded cubosomal gel: in vitro characterization, ex vivo permeation, and in vivo biodistribution studies. *Int J Nanomedicine*. 2020;15:9517. doi:10.2147/IJN.S277352
138. El Maghraby GM, Williams AC, Barry BW. Skin delivery of oestradiol from lipid vesicles: importance of liposome structure. *Int J Pharm*. 2000;204(1–2):159–169. doi:10.1016/S0378-5173(00)00493-2
139. Oh YK, Kim MY, Shin JY, et al. Skin permeation of retinol in Tween 20-based deformable liposomes: in-vitro evaluation in human skin and keratinocyte models. *J Pharm Pharmacol*. 2006;58(2):161–166. doi:10.1211/jpp.58.2.0002
140. Ahad A, Aqil M, Kohli K, Sultana Y, Mujeeb M, Ali A. Formulation and optimization of nanotransfersomes using experimental design technique for accentuated transdermal delivery of valsartan. *Nanomedicine*. 2012;8(2):237–249. doi:10.1016/j.nano.2011.06.004
141. Moawad FA, Ali AA, Salem HF. Nanotransfersomes-loaded thermosensitive in situ gel as a rectal delivery system of tizanidine HCl: preparation, in vitro and in vivo performance. *Drug Deliv*. 2017;24(1):252–260. doi:10.1080/10717544.2016.1245369
142. Abdulbaqi IM, Darwis Y, Abou Assi R, Khan NAK. Transethosomal gels as carriers for the transdermal delivery of colchicine: statistical optimization, characterization, and ex vivo evaluation. *Drug Des Devel Ther*. 2018;12:795. doi:10.2147/DDDT.S158018

143. Ahmed OA, Badr-Eldin SM. In situ misemgel as a multifunctional dual-absorption platform for nasal delivery of raloxifene hydrochloride: formulation, characterization, and in vivo performance. *Int J Nanomedicine*. 2018;13:6325. doi:10.2147/IJN.S181587
144. Almeida H, Amaral MH, Lobão P, Lobo JMS. Pluronic® F-127 and Pluronic Lecithin Organogel (PLO): main features and their applications in topical and transdermal administration of drugs. *J Pharm Pharmaceutical Sci*. 2012;15(4):592–605. doi:10.18433/J3HW2B
145. Patel KK, Kumar P, Thakkar HP. Formulation of niosomal gel for enhanced transdermal lopinavir delivery and its comparative evaluation with ethosomal gel. *AAPS pharmscitech*. 2012;13(4):1502–1510. doi:10.1208/s12249-012-9871-7
146. Salatin S, Barar J, Barzegar-Jalali M, Adibkia K, Milani MA, Jelvehgari M. Hydrogel nanoparticles and nanocomposites for nasal drug/vaccine delivery. *Arch Pharm Res*. 2016;39(9):1181–1192. doi:10.1007/s12272-016-0782-0
147. Ahmed OA, Fahmy U, Badr-Eldin SM, et al. Application of nanopharmaceutics for flibanserin brain delivery augmentation via the nasal route. *Nanomaterials*. 2020;10(7):1270. doi:10.3390/nano10071270
148. Das B, Sen SO, Maji R, Nayak AK, Sen KK. Transferosomal gel for transdermal delivery of risperidone: formulation optimization and ex vivo permeation. *J Drug Deliv Sci Technol*. 2017;38:59–71. doi:10.1016/j.jddst.2017.01.006
149. Garg BJ, Garg NK, Beg S, Singh B, Katare OP. Nanosized ethosomes-based hydrogel formulations of methoxsalen for enhanced topical delivery against vitiligo: formulation optimization, in vitro evaluation and preclinical assessment. *J Drug Target*. 2016;24(3):233–246. doi:10.3109/1061186X.2015.1070855
150. Mazzone F, Simons VE, van Geelen L, et al. In Vitro Biological Activity of Natural Products from the Endophytic Fungus Paraboeremia selaginellae against Toxoplasma gondii. *Antibiotics*. 2022;11(9):1176. doi:10.3390/antibiotics11091176
151. Abdellatif AA, Aldosari BN, Al-Subaiyel A, et al. Transethosomal Gel for the Topical Delivery of Celecoxib: formulation and Estimation of Skin Cancer Progression. *Pharmaceutics*. 2022;15(1):22. doi:10.3390/pharmaceutics15010022
152. Al-Rabia MW, Alhakamy NA, Ahmed OA, et al. Repurposing of sitagliptin-melittin optimized nanoformula against sars-cov-2; antiviral screening and molecular docking studies. *Pharmaceutics*. 2021;13(03):307. doi:10.3390/pharmaceutics13030307
153. Ng SW, Selvarajah GT, Hussein MZ, Yeap SK, Omar AR. In Vitro Evaluation of Curcumin-Encapsulated Chitosan Nanoparticles against Feline Infectious Peritonitis Virus and Pharmacokinetics Study in Cats. *Biomed Res Int*. 2020;2020:1–18. doi:10.1155/2020/3012198
154. Monavari SH, Bolouri B, Ebrahimi SA, Ataei-pirkooh A, Ataei-Pirkooh A. The inhibitory effect of Acyclovir loaded nano-niosomes against herpes simplex virus type-1 in cell culture. *Med J Islam Repub Iran*. 2014;28:99.
155. Shah J, Nair AB, Shah H, Jacob S, Shehata TM, Morsy MA. Enhancement in antinociceptive and anti-inflammatory effects of tramadol by transdermal proniosome gel. *Asian J Pharm Sci*. 2020;15(6):786–796. doi:10.1016/j.ajps.2019.05.001
156. Zakaria MY, Fayad E, Althobaiti F, Zaki I, Abu Almaaty AH. Statistical optimization of bile salt deployed nanovesicles as a potential platform for oral delivery of piperine: accentuated antiviral and anti-inflammatory activity in MERS-CoV challenged mice. *Drug Deliv*. 2021;28(1):1150–1165. doi:10.1080/10717544.2021.1934190
157. Badria FA, Abdelaziz AE, Hassan AH, Elgazar AA, Mazyed EA. Development of provesicular nanodelivery system of curcumin as a safe and effective antiviral agent: statistical optimization, in vitro characterization, and antiviral effectiveness. *Molecules*. 2020;25(23):5668. doi:10.3390/molecules25235668
158. El-Halim SMA, Mamdouh MA, El-Haddad AE, Soliman SM. Fabrication of anti-HSV-1 curcumin stabilized nanostructured proniosomal gel: molecular docking studies on thymidine kinase proteins. *Sci Pharm*. 2020;88(1):9. doi:10.3390/scipharm88010009
159. Brezáni V, Leláková V, Hassan ST, et al. Anti-infectivity against herpes simplex virus and selected microbes and anti-inflammatory activities of compounds isolated from Eucalyptus globulus labill. *Viruses*. 2018;10(7):360. doi:10.3390/v10070360
160. Mahmoud DB, Bakr MM, Al-Karmalawy AA, Moatasim Y, El Taweel A, Mostafa A. Scrutinizing the feasibility of nonionic surfactants to form isotropic bicelles of curcumin: a potential antiviral candidate against COVID-19. *AAPS PharmSciTech*. 2022;23(1):1–12. doi:10.1208/s12249-021-02197-2
161. Mathew D, Hsu W-L. Antiviral potential of curcumin. *J Funct Foods*. 2018;40:692–699. doi:10.1016/j.jff.2017.12.017
162. Bonfim CMD, Monteleoni LF, Calmon MDF, et al. Antiviral activity of curcumin-nanoemulsion associated with photodynamic therapy in vulvar cell lines transducing different variants of HPV-16. *Artif Cells, Nanomed Biotechnol*. 2020;48(1):515–524. doi:10.1080/21691401.2020.1725023
163. Ma Z, Wang N, He H, Tang X. Pharmaceutical strategies of improving oral systemic bioavailability of curcumin for clinical application. *J Controlled Release*. 2019;316:359–380. doi:10.1016/j.jconrel.2019.10.053
164. Mehanny M, Hathout RM, Geneidi AS, Mansour S. Exploring the use of nanocarrier systems to deliver the magical molecule; curcumin and its derivatives. *J Controlled Release*. 2016;225:1–30. doi:10.1016/j.jconrel.2016.01.018
165. Zhang L, Yang S, Wong LR, Xie H, Ho PC-L. In vitro and in vivo comparison of curcumin-encapsulated chitosan-coated poly (lactic-co-glycolic acid) nanoparticles and curcumin/hydroxypropyl-β-Cyclodextrin inclusion complexes administered intranasally as therapeutic strategies for Alzheimer's Disease. *Mol Pharm*. 2020;17(11):4256–4269. doi:10.1021/acs.molpharmaceut.0c00675
166. Prasad S, Tyagi AK, Aggarwal BB. Recent developments in delivery, bioavailability, absorption and metabolism of curcumin: the golden pigment from golden spice. *Cancer Res Treatment*. 2014;46(1):2–18. doi:10.4143/crt.2014.46.1.2
167. Wang Y-J, Pan M-H, Cheng A-L, et al. Stability of curcumin in buffer solutions and characterization of its degradation products. *J Pharm Biomed Anal*. 1997;15(12):1867–1876. doi:10.1016/S0731-7085(96)02024-9
168. Wang S, Chen P, Zhang L, Yang C, Zhai G. Formulation and evaluation of microemulsion-based in situ ion-sensitive gelling systems for intranasal administration of curcumin. *J Drug Target*. 2012;20(10):831–840. doi:10.3109/1061186X.2012.719230
169. Yu A, Wang H, Wang J, et al. Formulation optimization and bioavailability after oral and nasal administration in rabbits of puerarin-loaded microemulsion. *J Pharm Sci*. 2011;100(3):933–941. doi:10.1002/jps.22333
170. Al Asmari AK, Ullah Z, Tariq M, Fatani A. Preparation, characterization, and in vivo evaluation of intranasally administered liposomal formulation of donepezil. *Drug Des Devel Ther*. 2016;10:205.
171. Ryu EK, Choe YS, Lee K-H, Choi Y, Kim B-T. Curcumin and dehydrozingerone derivatives: synthesis, radiolabeling, and evaluation for β-amyloid plaque imaging. *J Med Chem*. 2006;49(20):6111–6119. doi:10.1021/jm0607193
172. Ravindranath V, Chandrasekhara N. Absorption and tissue distribution of curcumin in rats. *Toxicology*. 1980;16(3):259–265. doi:10.1016/0300-483X(80)90122-5
173. Pan M-H, Huang T-M, Lin J-K. Biotransformation of curcumin through reduction and glucuronidation in mice. *Drug Metabolism Disposition*. 1999;27(4):486–494.

174. Jiang F, Yu T, Liu X, Ding Z, Ma Z, Shi N. Biodistribution of curcumin and its derivatives new aspects for curcumin administration. *IEEE*. 2011;3878–3881.
175. Manca, M L, Peris J, Melis V, Lattuada D, et al. Nanoincorporation of Curcumin in Polymer-Glycerosomes and Evaluation of their In Vitro-In Vivo Suitability as Pulmonary Delivery Systems. *RSC Adv*. 2015;5:105149–105159. doi:10.1039/C5RA24032H
176. Avasarala S, Zhang F, Liu G, Wang R, London SD, London L. Curcumin modulates the inflammatory response and inhibits subsequent fibrosis in a mouse model of viral-induced acute respiratory distress syndrome. *PLoS One*. 2013;8(2):e57285. doi:10.1371/journal.pone.0057285
177. Zhang B, Swamy S, Balijepalli S, et al. Direct pulmonary delivery of solubilized curcumin reduces severity of lethal pneumonia. *FASEB J*. 2019;33(12):13294–13309. doi:10.1096/fj.201901047RR
178. Suresh MV, Wagner MC, Rosania GR, et al. Pulmonary administration of a water-soluble curcumin complex reduces severity of acute lung injury. *Am J Respir Cell Mol Biol*. 2012;47(3):280–287. doi:10.1165/rcmb.2011-0175OC
179. Dei Cas M, Ghidoni R. Dietary curcumin: correlation between bioavailability and health potential. *Nutrients*. 2019;11(9):2147. doi:10.3390/nu11092147
180. Thorne R, Pronk G, Padmanabhan V, Frey Ii W. Delivery of insulin-like growth factor-I to the rat brain and spinal cord along olfactory and trigeminal pathways following intranasal administration. *Neuroscience*. 2004;127(2):481–496. doi:10.1016/j.neuroscience.2004.05.029
181. Madane RG, Mahajan HS. Curcumin-loaded nanostructured lipid carriers (NLCs) for nasal administration: design, characterization, and in vivo study. *Drug Deliv*. 2016;23(4):1326–1334. doi:10.3109/10717544.2014.975382
182. Sintov AC. AmyloLipid Nanovesicles: a self-assembled lipid-modified starch hybrid system constructed for direct nose-to-brain delivery of curcumin. *Int J Pharm*. 2020;588:119725. doi:10.1016/j.ijpharm.2020.119725
183. Saber-Moghaddam N, Salari S, Hejazi S, et al. Oral nano-curcumin formulation efficacy in management of mild to moderate hospitalized coronavirus disease-19 patients: an open label nonrandomized clinical trial. *Phytotherapy Res*. 2021;35(5):2616–2623. doi:10.1002/ptr.7004